ARTICLE

doi:10.1038/nature13154

Synapse elimination and learning rules co-regulated by MHC class I H2-D^b

Hanmi Lee[1], Barbara K. Brott[1], Lowry A. Kirkby[2], Jaimie D. Adelson[1], Sarah Cheng[1], Marla B. Feller[2], Akash Datwani[1]† & Carla J. Shatz[1]

The formation of precise connections between retina and lateral geniculate nucleus (LGN) involves the activity-dependent elimination of some synapses, with strengthening and retention of others. Here we show that the major histocompatibility complex (MHC) class I molecule H2-D^b is necessary and sufficient for synapse elimination in the retinogeniculate system. In mice lacking both H2-K^b and H2-D^b ($K^bD^{b-/-}$), despite intact retinal activity and basal synaptic transmission, the developmentally regulated decrease in functional convergence of retinal ganglion cell synaptic inputs to LGN neurons fails and eye-specific layers do not form. Neuronal expression of just H2-D^b in $K^bD^{b-/-}$ mice rescues both synapse elimination and eye-specific segregation despite a compromised immune system. When patterns of stimulation mimicking endogenous retinal waves are used to probe synaptic learning rules at retinogeniculate synapses, long-term potentiation (LTP) is intact but long-term depression (LTD) is impaired in $K^bD^{b-/-}$ mice. This change is due to an increase in Ca^{2+}-permeable AMPA (α-amino-3-hydroxy-5-methyl-4-isoxazole propionic acid) receptors. Restoring H2-D^b to $K^bD^{b-/-}$ neurons renders AMPA receptors Ca^{2+} impermeable and rescues LTD. These observations reveal an MHC-class-I-mediated link between developmental synapse pruning and balanced synaptic learning rules enabling both LTD and LTP, and demonstrate a direct requirement for H2-D^b in functional and structural synapse pruning in CNS neurons.

Early in development, before photoreceptors function, retinal ganglion cells (RGCs) spontaneously generate correlated bursts of action potentials called 'retinal waves'[1–3]. Postsynaptic LGN neurons in turn are driven to fire in similar patterns[4,5], and this endogenous activity is even relayed further into the visual cortex[6]. Although there is consensus that retinal waves and correlated activity are needed for RGC synapse remodelling and segregation of RGC axons into eye-specific layers[7,8], little is known at the synaptic or molecular level about how natural patterns of activity are read out to drive elimination and structural remodelling before sensory experience. It is assumed that synaptic learning rules are present at retinogeniculate synapses, and that implementation of these rules ultimately leads either to synapse stabilization or elimination. Efforts to discover molecular mechanisms of developmental synapse elimination have implicated several unexpected candidates, all with links to the immune system, including neuronal pentraxins, Complement C1q and MHC class I family members[9–11]. However, it is not known whether any of these molecules regulate plasticity rules at developing synapses. Moreover, because germline knockout mice were examined in each of these examples, it is not known whether neuronal versus immune function is required for synapse elimination *in vivo*. Here we examine these questions and also test whether genetically restoring H2-D^b expression selectively to CNS neurons *in vivo* can rescue synapse elimination in mice that nevertheless lack an intact immune system.

Defective synapse elimination in LGN of $K^bD^{b-/-}$ mutant mice

MHC class I genes *H2-D^b* and *H2-K^b*, members of a polymorphic family of over 50, are expressed in LGN neurons[10] and were discovered in an unbiased screen *in vivo* for genes regulated by retinal waves: blocking this endogenous neural activity not only prevents RGC axonal remodelling[7], but also downregulates expression of MHCI messenger RNA[12]. Previous studies have suggested that MHCI molecules regulate synapse number in cultured neurons[13] and are needed for anatomical segregation of RGC axons into LGN layers *in vivo*[10,14]. To examine if H2-K^b and H2-D^b are involved in functional synapse elimination, whole-cell microelectrode recordings were made from individual neurons in wild-type or $K^bD^{b-/-}$ LGN slices (Fig. 1a)[15,16]. Adult mouse LGN neurons normally receive strong monosynaptic inputs from 1–3 RGC axons, but in development, many weak synaptic inputs are present. Most are eliminated between postnatal day 5 (P5) and P12 before eye opening, while the few remaining inputs strengthen, resulting in adult-like synaptic innervation by P24–P30 (ref. 15). By gradually increasing optic tract stimulation intensity, individual RGC axons with progressively higher firing thresholds can be recruited[15], generating a stepwise series of excitatory postsynaptic currents (EPSCs) recorded in each LGN neuron. For example, at P21 in wild type, only two steps are present (Fig. 1b), indicating that just two RGC axons provide input to this LGN neuron, as expected. In contrast, in $K^bD^{b-/-}$ LGN neurons, there are many EPSC steps (Fig. 1c), a pattern similar to that in much younger wild-type mice before synapse elimination[15,16].

To obtain more quantitative information, minimal stimulation was used to estimate single fibre strength (SF-AMPA)[17] (Methods and Extended Data Fig. 1a, b). On average, the amplitude of SF-AMPA in $K^bD^{b-/-}$ neurons is almost half that of wild type, and the cumulative probability distribution of EPSC amplitudes recorded from $K^bD^{b-/-}$ LGN neurons is also consistent with the presence of smaller sized EPSCs (Fig. 1d; note onset latency of SF-AMPA is similar in both genotypes (Extended Data Fig. 1c)). In contrast, maximal synaptic input (Max-AMPA) is not different between wild type and $K^bD^{b-/-}$ (Extended Data Fig. 1d). Fibre fraction, an index of how much each input contributes to total synaptic response[15] (Methods), is half as large in $K^bD^{b-/-}$ than wild type (Fig. 1e), consistent with the idea that the number of RGC synapses in $K^bD^{b-/-}$ LGN neurons is greater than in wild type. An alternative possibility—that differences can arise from altered probability of

[1]Departments of Biology and Neurobiology and Bio-X, James H. Clark Center, 318 Campus Drive, Stanford, California 94305, USA. [2]Department of Molecular and Cell Biology & Helen Wills Neuroscience Institute, University of California, Berkeley, California 94720, USA. †Present address: Sage Bionetworks, 1100 Fairview Avenue N., Seattle, Washington 98109, USA.

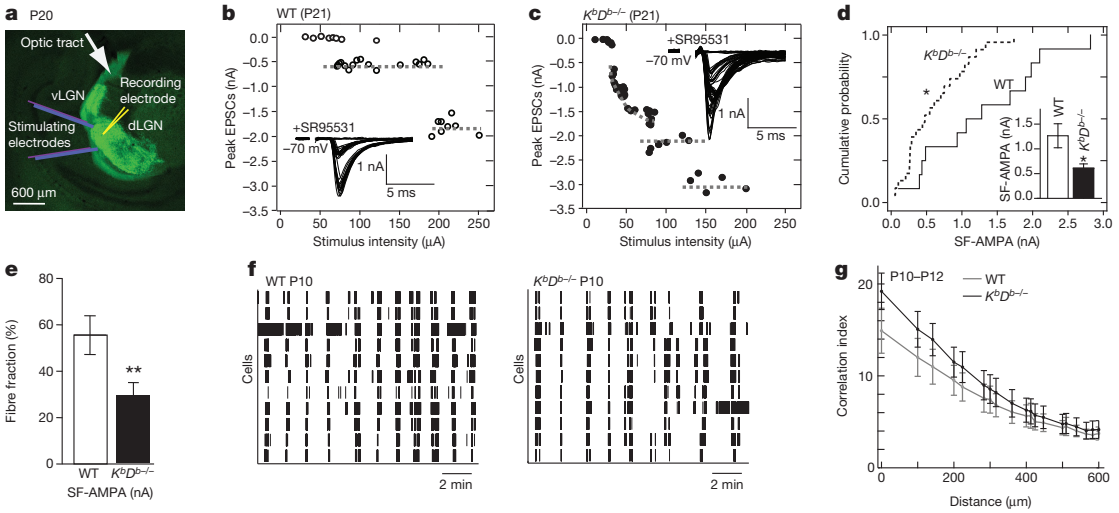

Figure 1 | Failure of retinogeniculate synapse elimination despite intact retinal waves in $K^bD^{b-/-}$. **a**–**e**, Impaired synapse elimination in $K^bD^{b-/-}$ mice at P20–P24. **a**, Slice preparation used for whole-cell recording from dLGN neurons and stimulation of retinal ganglion cell (RGC) axons in the optic tract. The retinogeniculate projection is visualized by injecting CTB AF488 (green) into the contralateral eye. **b**, **c**, EPSC amplitude versus optic tract stimulus intensity. Insets: example traces. **d**, Cumulative probability histograms of single fibre synaptic strength (SF-AMPA). Inset: mean ± s.e.m. for wild type (WT) ($n = 12/N = 6$); $K^bD^{b-/-}$ ($n = 23/N = 8$), $*P < 0.05$. **e**, Fibre fraction for wild type ($n = 12/N = 6$); $K^bD^{b-/-}$ ($n = 21/N = 8$), $**P < 0.01$, *t*-test for **d**, **e**. **f**, **g**, Intact retinal waves in $K^bD^{b-/-}$ at P10–P12. **f**, Raster plots of single-unit spike trains recorded from 10 representative RGCs during retinal waves. **g**, Correlation indices versus inter-electrode distance for all cell pairs for wild type ($N = 5$) versus $K^bD^{b-/-}$ ($N = 6$). Data correspond to mean values of medians from individual data sets and error bars represent s.e.m. n = cells/N = animals.

release—is unlikely because paired-pulse ratio, an index of presynaptic release probability, is similar in wild type and $K^bD^{b-/-}$ at a variety of stimulus intervals (Extended Data Fig. 1e–h). Together, these experiments, which directly measure the functional status of synaptic innervation, demonstrate that either or both H2-K^b and H2-D^b are required for retinogeniculate synapse elimination.

Intact retinal wave activity in $K^bD^{b-/-}$ mice

Many previous studies have shown that retinogeniculate synapse elimination and eye-specific segregation in LGN fail if retinal waves are blocked or perturbed[2,7,8]. Thus, waves could be absent or abnormal in $K^bD^{b-/-}$ mice. To examine this possibility, waves were recorded using a multi-electrode array to monitor action potential activity from many ganglion cells in $K^bD^{b-/-}$ or wild-type retinas between P5–P12, the peak period of extensive RGC synapse remodelling requiring waves. The spatio-temporal pattern of waves in $K^bD^{b-/-}$ is indistinguishable from wild type (Fig. 1f and Extended Data Fig. 2a–e). Moreover, the correlation index between all RGC pairs, a measure of the distance over which cells fire together[1,3,18], is almost identical (Fig. 1g and Extended Data Fig. 2a). Retinal wave activity also transitioned normally from cholinergic-dependent stage II (P5–P8) to glutamatergic-dependent stage III (P10–P12) (Extended Data Fig. 2a–e)[8]. After eye opening, vision in $K^bD^{b-/-}$ mice is also normal[14]. Thus, synapse elimination and eye-specific segregation fail to occur despite intact retinal activity patterns in $K^bD^{b-/-}$ mice, indicating that one or both of these MHCI proteins acts downstream of activity to drive synapse remodelling.

Neuronal H2-D^b rescues elimination and segregation

H2-D^b and H2-K^b are also critical for immune function and CD8 T-cell development[19]. Both MHCI molecules are expressed in LGN during the period of retinogeniculate synaptic refinement, with H2-D^b expressed at a higher level than H2-K^b (refs 10, 14). To separate a contribution of the immune system, and to examine if neuronal expression is sufficient for synapse elimination, H2-D^b expression was restored exclusively to neurons by crossing $K^bD^{b-/-}$ mice to $NSED^{b+}$ mice in which H2-D^b expression is regulated under the neuron-specific enolase (NSE) promoter[20]. 'Rescued' offspring littermates have H2-D^b expression restored to CNS neurons while the rest of the body remains $K^bD^{b-/-}$ ($K^bD^{b-/-}$;$NSED^{b+}$); 'control' littermates ($K^bD^{b-/-}$;$NSED^{b-}$) lack H2-K^b and H2-D^b throughout the body (Extended Data Fig. 3a). Genomic rescue, as well as low but highly significant levels of H2-D^b mRNA ($P = 0.0001$) and protein can be detected in $K^bD^{b-/-}$;$NSED^{b+}$ thalamus at P10 (Extended Data Fig. 3b–e). In contrast, no H2-D^b can be detected in spleen, gut or liver, with little if any expression in retina, hippocampus and cortex of $K^bD^{b-/-}$;$NSED^{b+}$ mice.

In $K^bD^{b-/-}$;$NSED^{b+}$ LGN neurons, only 1–2 EPSC steps could be evoked in response to increasing optic tract stimulus intensity (Fig. 2a), similar to the mature wild-type innervation pattern (see Fig. 1b) but very different from littermate $K^bD^{b-/-}$;$NSED^{b-}$ controls (Fig. 2b). Minimal stimulation also revealed an increase in SF-AMPA strength (Fig. 2c and Extended Data Figs 1c and 4b). Max-AMPA is similar between these genotypes (Extended Data Fig. 4a); thus fibre fraction in $K^bD^{b-/-}$;$NSED^{b+}$ LGN neurons is 56%, versus 25% in $K^bD^{b-/-}$;$NSED^{b-}$ neurons (Fig. 2d)—also markedly similar to wild type fibre fraction (see Fig. 1e). Thus, expression of H2-D^b in neurons rescues RGC synapse elimination in LGN of $K^bD^{b-/-}$ mice close to wild-type levels.

The formation of the adult anatomical pattern of eye-specific segregation in the LGN involves synapse elimination: initially intermixed retinal ganglion cell axons from the right and left eyes remodel, eventually restricting their terminal arborizations to the appropriate LGN layer[21,22]. To examine whether eye-specific segregation in the LGN is also rescued, anatomical tract tracing methods[14,23] were used at P34, an age chosen because it is more than 3 weeks after segregation is normally complete as assessed anatomically. The retinogeniculate projections in LGN of $K^bD^{b-/-}$;$NSED^{b+}$ mice appear almost indistinguishable from wild type, both in eye-specific pattern (Fig. 2e) and in per cent ipsi-contra overlap (Fig. 2f and Extended Data Fig. 5a, b). Segregation is impaired in control $K^bD^{b-/-}$;$NSED^{b-}$ littermates (Fig. 2e), as expected from previous studies of $K^bD^{b-/-}$ mice[14]. These anatomical results support the electrophysiological studies above and strongly suggest that both RGC synapse elimination and eye-specific segregation require neuronal H2-D^b.

Impaired LTD with natural activity patterns

Synapse elimination is thought to involve cellular processes leading to synaptic weakening such as LTD[24,25]; conversely LTP-like mechanisms

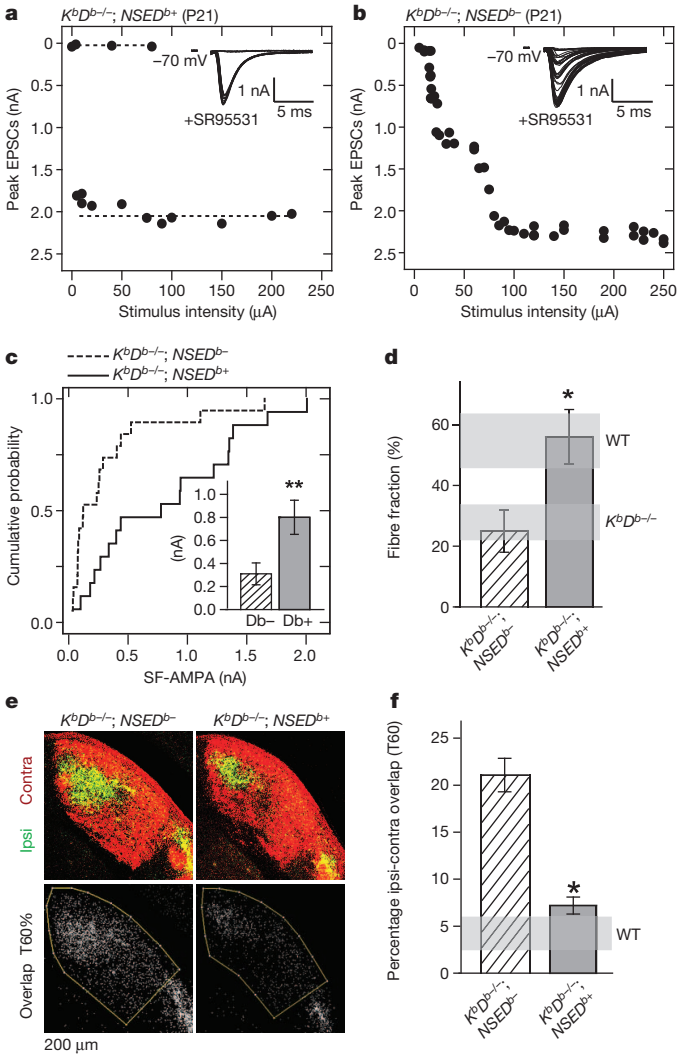

Figure 2 | H2-D^b expression in neurons rescues synapse elimination and eye-specific segregation in $K^bD^{b-/-}$ LGN. **a**–**d**, Rescue of synapse elimination at P20–P24. **a**, **b**, EPSC amplitudes versus optic tract stimulus intensity. Insets: example traces. **c**, Cumulative probability histogram of SF-AMPA. Inset: mean ± s.e.m. for control: D^{b-} ($K^bD^{b-/-}$;$NSED^{b-}$, $n = 19/N = 5$). Rescue: D^{b+} ($K^bD^{b-/-}$;$NSED^{b+}$, $n = 17/N = 7$), $^{**}P < 0.01$. **d**, Fibre fraction is also rescued in $K^bD^{b-/-}$;$NSED^{b+}$ ($n = 16/N = 7$) compared to $K^bD^{b-/-}$;$NSED^{b-}$ ($n = 18/N = 5$), $^{*}P < 0.05$, Mann–Whitney *U*-test for **c**, **d**. Horizontal grey bars delineate Fig. 1e data (mean ± s.e.m.). **e**, **f**, Rescue of eye-specific segregation in $K^bD^{b-/-}$;$NSED^{b+}$ at P34. **e**, Top: coronal sections of dLGN showing pattern of retinogeniculate projections from the ipsilateral (green) and contralateral (red) eyes. Bottom: region of ipsi-contra pixel (white) overlap between the two channels at 60% intensity threshold (T60%). **f**, Percentage of dLGN area occupied by ipsi-contra overlap. mean ± s.e.m. for $K^bD^{b-/-}$;$NSED^{b-}$ ($N = 3$) and $K^bD^{b-/-}$;$NSED^{b+}$ ($N = 4$) (T60%) ($^{*}P < 0.05$, two way ANOVA) (see Extended Data Fig. 5). Horizontal grey bar indicates wild-type value at T60% (from ref. 14). n = cells/N = animals.

are postulated for synaptic strengthening and stabilization[26,27]. In addition, spike-timing-dependent mechanisms are crucial in *Xenopus* tectum for visually driven tuning of receptive fields[28]. In mammalian LGN, LTP[29] or LTD[30] can be induced at retinogeniculate synapses using 100 Hz optic tract stimulation, which is far from the endogenous bursting patterns generated by retinal waves (Fig. 1f, g)[1–4]. However, realistic patterns of optic tract stimulation mimicking waves, paired with postsynaptic depolarization of LGN neurons, have also been used; results revealed a synaptic learning rule that generates LTP when pre- and postsynaptic activity are coincident[31,32], but LTD when presynaptic optic tract activity precedes postsynaptic LGN depolarization within a broad window corresponding to the 60–90 s duty cycle of retinal waves (Fig. 3a–c and Extended Data Fig. 2b)[31]. Moreover, using these timing patterns in conjunction with optogenetic stimulation of retina is sufficient either to drive or prevent segregation of RGC axons depending on the pattern[33]. To determine whether synaptic learning rules based on natural activity patterns are altered at $K^bD^{b-/-}$ retinogeniculate synapses, perforated patch recordings were made in LGN slices from wild type versus $K^bD^{b-/-}$ at P8–P13, the relevant period when extensive synapse elimination and eye-specific segregation are actually occurring. First, paired-pulse stimulation was used to examine release probability: the same amount of synaptic depression was observed in wild-type and $K^bD^{b-/-}$ mice, indicating similar probabilities (Extended Data Fig. 6). Next, synchronous activity patterns were used, in which 10 Hz optic tract stimulation was paired with LGN depolarization (Fig. 3a, b: 0 ms latency), generating 10–20 Hz bursts of action potentials in LGN neurons mimicking retinal waves[4,5]. In wild type, synchronous stimulation induced LTP (Fig. 3d, f; 117 ± 8% over baseline; $P < 0.001$). In $K^bD^{b-/-}$ LGN neurons, the same protocol elicited LTP indistinguishable from wild type (Fig. 3e, f).

In contrast, induction using asynchronous activity patterns reveals a defect in LTD. In wild type, when optic tract stimulation precedes LGN neuron depolarization by 1.1 s (Fig. 3a, c: 1,100 ms latency), LTD results (Fig. 3g, i: 12% decrease from baseline; $P < 0.001$). In contrast, in $K^bD^{b-/-}$, the same induction protocol failed to induce synaptic depression; if anything, a slight but significant potentiation was seen (Fig. 3h, i: 5% increase from baseline; $P < 0.005$). Thus, whereas LTD using asynchronous pre- and postsynaptic activity patterns is a robust feature of wild-type retinogeniculate synapses during the period of synapse elimination and eye-specific layer formation, it seems to be absent in $K^bD^{b-/-}$ mice. This impairment is consistent with the failure of synapse elimination and axonal remodelling in $K^bD^{b-/-}$ mice.

Ca^{2+}-permeable AMPA receptors at $K^bD^{b-/-}$ synapses

Impaired LTD in $K^bD^{b-/-}$ mice could be due to altered regulation of NMDA (*N*-methyl-D-aspartate)-receptor-mediated synaptic responses, as LTP and LTD are known to be dependent on NMDA receptors at a variety of synapses[26]. Surprisingly, the NMDA/AMPA ratio was not different between genotypes (Extended Data Fig. 7a, b). However, the kinetics of I_{AMPA} recorded in $K^bD^{b-/-}$ LGN neurons are markedly prolonged compared to wild type (Fig. 4a–d). The slowed decay in $K^bD^{b-/-}$ EPSCs is unlikely to be due to different peak I_{AMPA} amplitudes ($P > 0.1$; Fig. 4d), but could occur if there were greater Ca^{2+} influx through AMPA receptors.

Ca^{2+}-permeable AMPA (CP-AMPA) receptors are blocked selectively by bath-applying the specific antagonist NASPM, a synthetic homologue of joro spider toxin[34]. Indeed in $K^bD^{b-/-}$ LGN neurons, 100 μM NASPM blocked 40% of the current recorded at −70 mV but only 20% in wild type (Fig. 4e and Extended Data Fig. 7c), confirming a two-fold increase in CP-AMPA receptor-mediated currents in $K^bD^{b-/-}$ neurons. Another diagnostic feature of CP-AMPA receptors is rectification in the current–voltage (*I–V*) relationship when spermine is present in the internal recording solution[34–36]. In wild type, the *I–V* relationship is linear. However in $K^bD^{b-/-}$ LGN neurons, rectification is very prominent (Fig. 4f, g and Extended Data Fig. 7d) but can be linearized close to wild-type levels by bath application of NASPM (Fig. 4f, g), indicating that the prominent *I–V* rectification in $K^bD^{b-/-}$ arises from an increase in CP-AMPA receptors.

Differences in composition of GluR subunits are known to modulate AMPA receptor Ca^{2+} permeability, and tetramers containing GluR2 confer Ca^{2+} impermeability[35]. Indeed, the ratio of GluR1 to GluR2, the most prevalent subunits[35,37,38], is slightly increased in developing thalamus from $K^bD^{b-/-}$ mice (30% increase in $K^bD^{b-/-}$, $P = 0.07$; Extended Data Fig. 7e). The thalamus is highly heterogeneous, so we also examined cortical neuronal cultures: the ratio of GluR1 to GluR2 is also significantly increased (230% increase in $K^bD^{b-/-}$; $P = 0.03$; Extended Data Fig. 7f). Elevated levels of GluR1 subunits suggest that AMPA receptors in $K^bD^{b-/-}$ are more likely to be composed of GluR1 homomers,

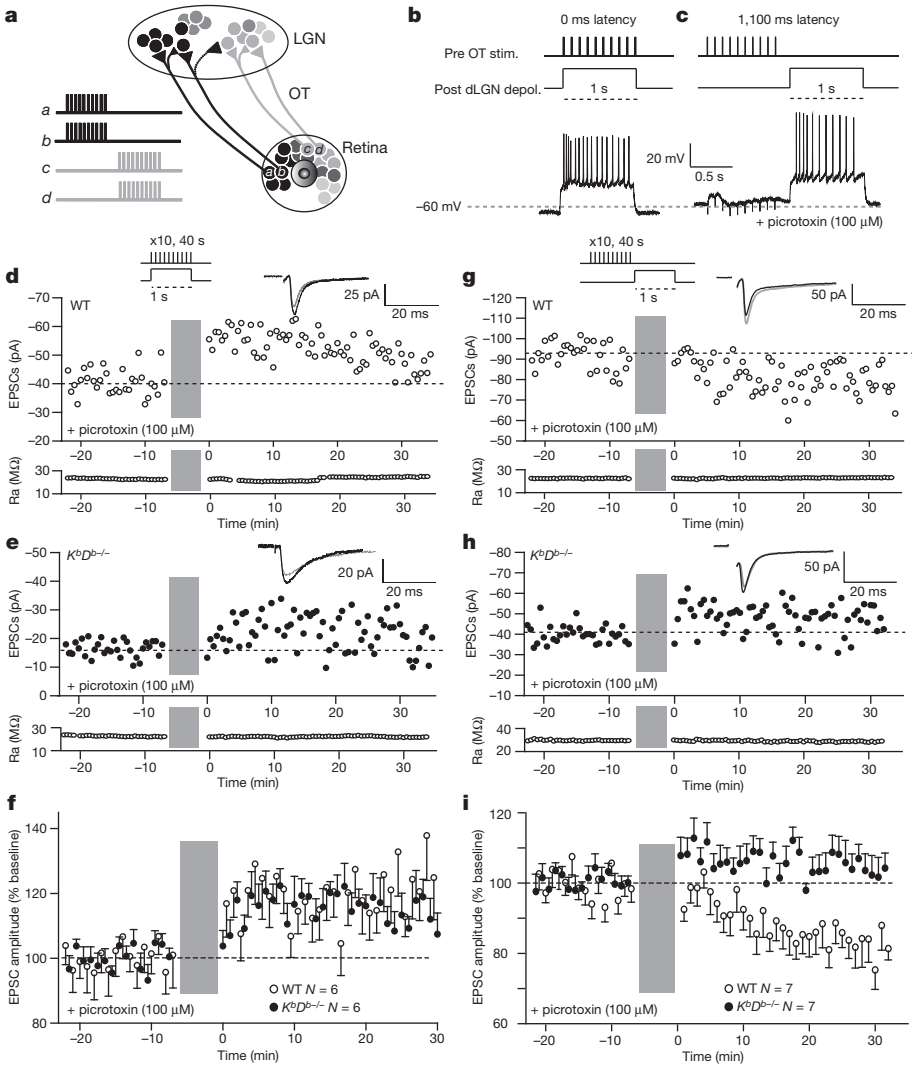

Figure 3 | Impaired LTD but intact LTP at retinogeniculate synapses in $K^bD^{b-/-}$ induced with natural activity patterns. a, Diagram illustrating basis for timing-dependent plasticity at developing retinogeniculate synapses. Spontaneous retinal waves propagate from '*a*, *b*' towards '*c*, *d*'; neighbouring RGCs fire synchronously but asynchronously with respect to RGCs located elsewhere. Waves drive action potentials in postsynaptic LGN neurons with varying time delays between pre- and postsynaptic activity. Ages P8–13 were studied. **b**, **c**, Top: conditioning protocol for LTP (0 ms latency; **b**) or LTD (1,100 ms latency; **c**). Bottom: example membrane potential changes recorded in LGN neuron during conditioning protocol. OT, optic tract. **d**–**f**, Intact LTP in $K^bD^{b-/-}$. Single experiment showing LTP in wild type (**d**) and $K^bD^{b-/-}$ (**e**). EPSC peak amplitude versus time. **f**, Summary of all 0 ms latency experiments: EPSC peak amplitude (% change from baseline) versus time ($n = 6/N = 6$ for each; $P > 0.1$, *t*-test). **g**–**i**, Deficient LTD in $K^bD^{b-/-}$. Single experiment for wild type (**g**) and $K^bD^{b-/-}$ (**h**). EPSC peak amplitude versus time. **i**, Summary of all 1,100 ms latency experiments: EPSC peak amplitude (% change from baseline) versus time ($n = 7/N = 7$ for each; $P < 0.01$, *t*-test). Grey bars indicate induction period. Insets: average EPSCs (30 traces) before (grey) and after (black) induction. **f**, **i**, 1 min data binning. Ra, access resistance (MΩ). n = cells/N = animals.

yielding increased Ca^{2+} permeability. Together, results point to an increase in CP-AMPA receptors in $K^bD^{b-/-}$ mice. Similar increases in CP-AMPA receptors at other synapses are known to shift synaptic learning rules away from LTD and towards LTP[39,40]. If so, the deficit in LTD observed with the asynchronous pairing protocol (Fig. 3c, i) in $K^bD^{b-/-}$ LGN should be rescued using NASPM to block CP-AMPA receptors—just what is observed (Extended Data Fig. 8).

Neuronal H2-D^b rescues synaptic function and LTD

If H2-D^b affects synapse elimination by regulating properties of AMPA receptors, then retinogeniculate EPSCs should be rescued to wild type in the LGN of $K^bD^{b-/-}$;$NSED^{b+}$ mice. Indeed, the kinetics of I_{AMPA} are significantly faster in $K^bD^{b-/-}$;$NSED^{b+}$ LGN neurons compared to $K^bD^{b-/-}$;$NSED^{b-}$ LGN neurons (Fig. 5a–c and Extended Data Fig. 9a), indicating a decrease in Ca^{2+}-permeable AMPA receptors. Accordingly, NASPM-dependent inhibition of I_{AMPA} is only 20% in $K^bD^{b-/-}$;$NSED^{b+}$, significantly reduced from the 40% inhibition observed in littermate $K^bD^{b-/-}$;$NSED^{b-}$ mice (Fig. 5d and Extended Data Fig. 9a). Moreover, the *I*–*V* relationship is linearized in $K^bD^{b-/-}$;$NSED^{b+}$ LGN neurons when spermine is present in the internal recording solution, and bath application of NASPM has little additional effect ($P > 0.5$ at +40 mV), similar to wild type (Fig. 5e and Extended Data Fig. 9b). Because the Ca^{2+} permeability of AMPA receptors is close to wild-type levels in $K^bD^{b-/-}$;$NSED^{b+}$ LGN, it is possible that LTD is also rescued. Indeed, the same asynchronous activity pattern that failed to induce LTD in $K^bD^{b-/-}$ (Fig. 3) induces robust LTD (15%; $P < 0.001$) in $K^bD^{b-/-}$;$NSED^{b+}$ neurons, similar to wild type (Fig. 5f, g). Together, these observations suggest that restoring expression of H2-D^b in neurons is sufficient to rescue LTD at retinogeniculate synapses via decreasing the Ca^{2+} permeability of AMPA receptors.

Discussion

A major finding of this study is that the link between activity-dependent synapse pruning during development, and regulation of LTD and CP-AMPA

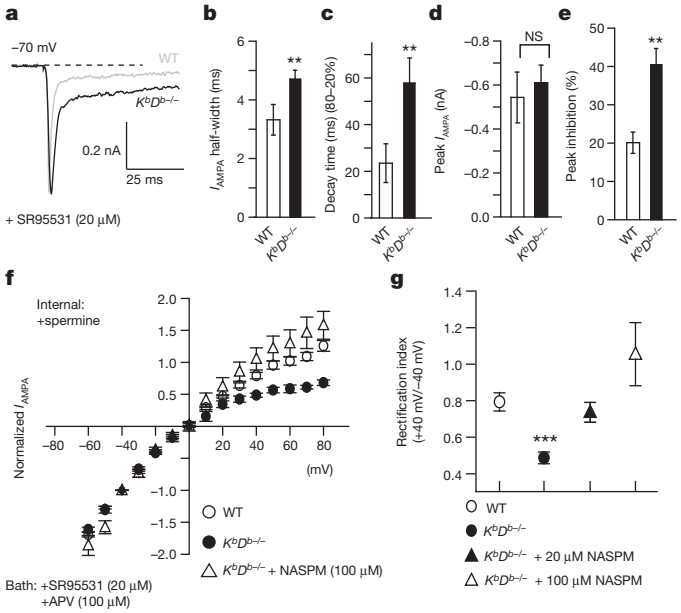

Figure 4 | Increased Ca^{2+}-permeable AMPA receptors at retinogeniculate synapses in $K^bD^{b-/-}$ LGN. **a–d**, Prolonged decay kinetics of I_{AMPA} in $K^bD^{b-/-}$ mice. **a**, Average I_{AMPA} (5–10 EPSCs) for wild-type versus $K^bD^{b-/-}$ LGN neurons. I_{AMPA} half-width (ms) (**b**), I_{AMPA} decay time (ms) (**c**) and peak amplitude (nA) (**d**) for wild type versus $K^bD^{b-/-}$ (WT, $n = 16/N = 4$; $K^bD^{b-/-}$, $n = 22/N = 5$). **e**, Increased per cent inhibition of peak I_{AMPA} by NASPM (100 μM) in $K^bD^{b-/-}$ ($n = 13/N = 4$) versus wild type ($n = 9/N = 3$) (**$P < 0.01$; NS, not significant; Mann–Whitney *U*-test for **b**, **c**). **f**, I_{AMPA} *I–V* curves (normalized to −40 mV). **g**, Rectification index for wild type ($n = 14/N = 3$), $K^bD^{b-/-}$ ($n = 9/N = 3$), $K^bD^{b-/-}$ +20 μM NASPM ($n = 16/N = 4$) or $K^bD^{b-/-}$ +100 μM NASPM ($n = 6/N = 2$) (***$P < 0.001$ for wild type versus $K^bD^{b-/-}$; $P > 0.05$ for wild type versus $K^bD^{b-/-}$ +NASPM (20 or 100 μM), Mann–Whitney *U*-test). Ages studied: P8–P13. Also, see Extended Data Fig. 7. n = cells/N = animals.

receptors, requires neuronal MHCI function. It is notable that synapse elimination fails despite the fact that retinal waves and retinogeniculate basal synaptic transmission are intact. The persistence of multiple innervation in $K^bD^{b-/-}$ LGN neurons is highly reminiscent of the immature synaptic connectivity in LGN of younger wild-type mice[15], as well as of abnormal connectivity observed in LGNs of dark-reared or tetrodotoxin-treated wild-type mice[16]. Together, these considerations indicate that H2-D^b and H2-K^b act downstream of neural activity. In studying synaptic plasticity at retinogeniculate synapses, we imposed plasticity induction protocols that mimic natural patterns of spiking activity present in the retinogeniculate system during synapse elimination and eye-specific segregation. Our observation that in $K^bD^{b-/-}$ mice LTD is impaired while LTP is intact can explain the failure in retinogeniculate synapse elimination: if synapses cannot undergo weakening, then they cannot be eliminated. Because immunostaining for MHCI proteins H2-D^b and H2-K^b is co-localized with synaptic markers in array tomography[14] and at synapses in immuno-electron microscopy[14,41], these observations also argue strongly that H2-D^b and/or H2-K^b at synapses regulate mechanisms of LTD, which in turn are required for synapse elimination. It would be useful to know whether other molecules implicated in RGC synapse elimination such as C1q (ref. 9), which co-localizes with H2-D^b and H2-K^b at synapses[14], also alter LTD or instead act downstream of MHCI to target already weakened synapses for removal.

The rescue experiments performed here indicate that a single MHCI molecule—H2-D^b, when expressed in neurons—is sufficient for functional synapse elimination and anatomical eye-specific segregation in the LGN. By crossing $K^bD^{b-/-}$ mice to $NSED^b$ transgenic mice, expression of H2-D^b alone was restored to neurons but not elsewhere in the body, rescuing LTD, functional synapse elimination, Ca^{2+}-impermeable AMPA receptors and structural remodelling at retinogeniculate synapses. Notably, these brain phenotypes are rescued even though the immune system is still impaired in $K^bD^{b-/-}$;$NSED^{b+}$ mice. Until this experiment, it was not known if any one MHCI molecule is sufficient either *in vitro* or *in vivo*, nor has it been possible to separate the general effects of immune compromise from the absence of H2-D^b and/or H2-K^b in neurons. Together, our observations argue for a key role for H2-D^b in reading out endogenous activity patterns into a lasting structural framework. In the human genome, as in mice, the MHCI (HLA) locus is large and highly polymorphic. Recent genome-wide association studies have consistently linked specific single nucleotide polymorphisms in MHCI to schizophrenia[42,43]. Our observations offer possible mechanistic insight: alterations in expression levels of specific MHCI molecules at neuronal synapses could trigger changes in activity-dependent plasticity and synaptic pruning during critical periods of human development, generating lasting alterations in circuits and behaviour.

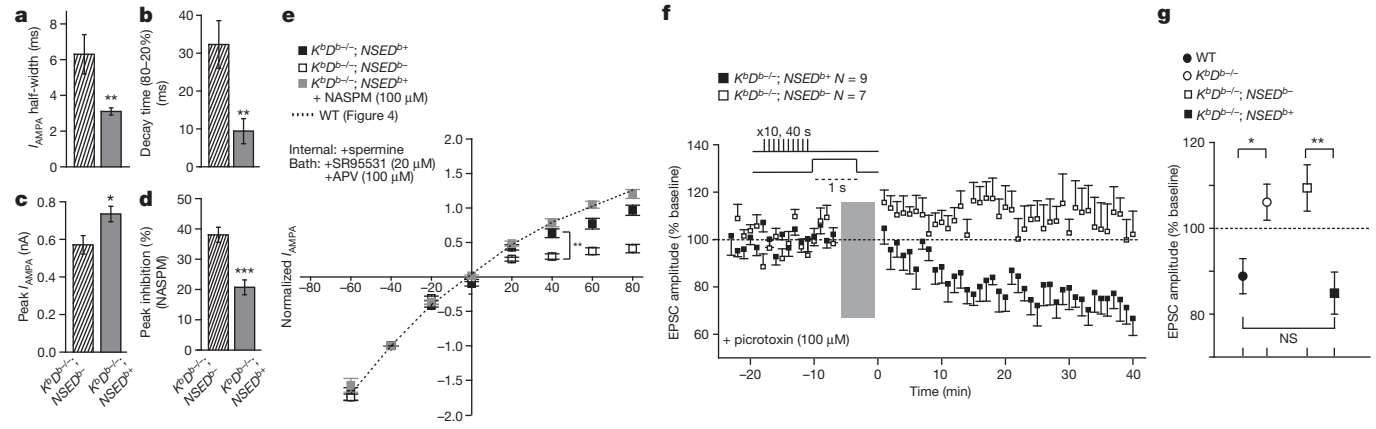

Figure 5 | Neuronal expression of H2-D^b restores Ca^{2+}-impermeable AMPA receptors and rescues LTD. **a–c**, I_{AMPA} half-width (ms) (**a**), I_{AMPA} decay time (ms) (**b**), and peak amplitude (nA) (**c**) for $K^bD^{b-/-}$;$NSED^{b-}$ ($n = 9/N = 2$) and $K^bD^{b-/-}$;$NSED^{b+}$ ($n = 11/N = 4$). **d**, Reduced per cent inhibition of peak I_{AMPA} by NASPM (100 μM) in $K^bD^{b-/-}$;$NSED^{b+}$ ($n = 10/N = 3$) compared to $K^bD^{b-/-}$;$NSED^{b-}$ ($n = 8/N = 2$); *$P < 0.05$, **$P < 0.01$, ***$P < 0.001$, Mann–Whitney *U*-test for **a–d**. **e**, Rescue of I_{AMPA} linear *I–V* relationship in $K^bD^{b-/-}$;$NSED^{b+}$ LGN. Rectification index at +40 mV for $K^bD^{b-/-}$;$NSED^{b-}$ ($n = 11/N = 3$) and $K^bD^{b-/-}$;$NSED^{b+}$ ($n = 13/N = 5$) shows significant difference (**$P < 0.005$); $K^bD^{b-/-}$;$NSED^{b+}$ (+NASPM) ($n = 7/N = 3$) is not significantly different to $K^bD^{b-/-}$;$NSED^{b+}$ ($P > 0.05$), Mann–Whitney *U*-test. See also Extended Data Fig. 9. mean ± s.e.m. **f**, **g**, LTD rescued in $K^bD^{b-/-}$;$NSED^{b+}$ LGN neurons. **f**, Ensemble average of all experiments at P8–9 (see Fig. 3). Grey bar indicates LTD induction period. 1 min data binning. **g**, Average per cent change (mean ± s.e.m.) for wild type ($N = 7$), $K^bD^{b-/-}$ ($N = 7$), $K^bD^{b-/-}$;$NSED^{b-}$ ($N = 7$) and $K^bD^{b-/-}$;$NSED^{b+}$: ($N = 9$). *$P < 0.05$, **$P < 0.01$, NS, not significant, *t*-test. P8–13 ages studied. n = cells/N = animals.

METHODS SUMMARY

All experimental protocols were approved by Stanford University Animal Care and Use Committees. $K^bD^{b-/-}$ mice were provided by H. Ploegh[19] and $NSED^{b+}$ mice by M. B. A. Oldstone[20]. These mice were maintained on C57BL/6 backgrounds. Crosses of these two lines generated $K^bD^{b-/-}$;$NSED^{b+}$ mice plus littermate controls. Electrophysiological recordings were made from LGN neurons by cutting parasagittal brain slices containing dorsal lateral geniculate nucleus (dLGN) and optic tract; synaptic transmission and degree of innervation was assessed as previously described[15]. For plasticity experiments at retinogeniculate synapses, perforated patch-clamp technique and induction protocols with natural activity patterns were used[31]. Multi-electrode array recordings of retinal waves and anatomical labelling of retinogeniculate projections to determine status of eye-specific segregation were carried out according to ref. 18 and ref. 14. Pharmacological investigation of CP-AMPA receptors was carried out according to ref. 34. All experiments were conducted and analysed blind to genotype except in Fig. 4 (genotype was obvious to experimenter because of phenotype). Sample sizes were chosen for each experiment to reach statistical significance (P value equal to or less than 0.05; details given in Methods and figure legends).

Online Content Any additional Methods, Extended Data display items and Source Data are available in the online version of the paper; references unique to these sections appear only in the online paper.

Received 18 February 2013; accepted 13 February 2014.
Published online 30 March 2014.

1. Meister, M., Wong, R. O., Baylor, D. A. & Shatz, C. J. Synchronous bursts of action potentials in ganglion cells of the developing mammalian retina. *Science* **252,** 939–943 (1991).
2. Feller, M. B., Wellis, D. P., Stellwagen, D., Werblin, F. S. & Shatz, C. J. Requirement for cholinergic synaptic transmission in the propagation of spontaneous retinal waves. *Science* **272,** 1182–1187 (1996).
3. Wong, R. O., Meister, M. & Shatz, C. J. Transient period of correlated bursting activity during development of the mammalian retina. *Neuron* **11,** 923–938 (1993).
4. Mooney, R., Penn, A. A., Gallego, R. & Shatz, C. J. Thalamic relay of spontaneous retinal activity prior to vision. *Neuron* **17,** 863–874 (1996).
5. Weliky, M. & Katz, L. C. Correlational structure of spontaneous neuronal activity in the developing lateral geniculate nucleus *in vivo*. *Science* **285,** 599–604 (1999).
6. Ackman, J. B., Burbridge, T. J. & Crair, M. C. Retinal waves coordinate patterned activity throughout the developing visual system. *Nature* **490,** 219–225 (2012).
7. Penn, A. A., Riquelme, P. A., Feller, M. B. & Shatz, C. J. Competition in retinogeniculate patterning driven by spontaneous activity. *Science* **279,** 2108–2112 (1998).
8. Huberman, A. D., Feller, M. B. & Chapman, B. Mechanisms underlying development of visual maps and receptive fields. *Annu. Rev. Neurosci.* **31,** 479–509 (2008).
9. Stevens, B. *et al.* The classical complement cascade mediates CNS synapse elimination. *Cell* **131,** 1164–1178 (2007).
10. Huh, G. S. *et al.* Functional requirement for class I MHC in CNS development and plasticity. *Science* **290,** 2155–2159 (2000).
11. Bjartmar, L. *et al.* Neuronal pentraxins mediate synaptic refinement in the developing visual system. *J. Neurosci.* **26,** 6269–6281 (2006).
12. Corriveau, R. A., Huh, G. S. & Shatz, C. J. Regulation of class I MHC gene expression in the developing and mature CNS by neural activity. *Neuron* **21,** 505–520 (1998).
13. Glynn, M. W. *et al.* MHCI negatively regulates synapse density during the establishment of cortical connections. *Nature Neurosci.* **14,** 442–451 (2011).
14. Datwani, A. *et al.* Classical MHCI molecules regulate retinogeniculate refinement and limit ocular dominance plasticity. *Neuron* **64,** 463–470 (2009).
15. Chen, C. & Regehr, W. G. Developmental remodeling of the retinogeniculate synapse. *Neuron* **28,** 955–966 (2000).
16. Hooks, B. M. & Chen, C. Distinct roles for spontaneous and visual activity in remodeling of the retinogeniculate synapse. *Neuron* **52,** 281–291 (2006).
17. Stevens, C. F. & Wang, Y. Changes in reliability of synaptic function as a mechanism for plasticity. *Nature* **371,** 704–707 (1994).
18. Torborg, C. L., Hansen, K. A. & Feller, M. B. High frequency, synchronized bursting drives eye-specific segregation of retinogeniculate projections. *Nature Neurosci.* **8,** 72–78 (2005).
19. Vugmeyster, Y. *et al.* Major histocompatibility complex (MHC) class I $K^bD^{b-/-}$ deficient mice possess functional $CD8^+$ T cells and natural killer cells. *Proc. Natl Acad. Sci. USA* **95,** 12492–12497 (1998).
20. Rall, G. F., Mucke, L. & Oldstone, M. B. Consequences of cytotoxic T lymphocyte interaction with major histocompatibility complex class I-expressing neurons *in vivo*. *J. Exp. Med.* **182,** 1201–1212 (1995).
21. Shatz, C. J. & Kirkwood, P. A. Prenatal development of functional connections in the cat's retinogeniculate pathway. *J. Neurosci.* **4,** 1378–1397 (1984).
22. Shatz, C. J. Emergence of order in visual system development. *Proc. Natl Acad. Sci. USA* **93,** 602–608 (1996).
23. Torborg, C. L. & Feller, M. B. Unbiased analysis of bulk axonal segregation patterns. *J. Neurosci. Methods* **135,** 17–26 (2004).
24. Zhou, Q., Homma, K. J. & Poo, M. M. Shrinkage of dendritic spines associated with long-term depression of hippocampal synapses. *Neuron* **44,** 749–757 (2004).
25. Bastrikova, N., Gardner, G. A., Reece, J. M., Jeromin, A. & Dudek, S. M. Synapse elimination accompanies functional plasticity in hippocampal neurons. *Proc. Natl Acad. Sci. USA* **105,** 3123–3127 (2008).
26. Malenka, R. C. & Bear, M. F. LTP and LTD: an embarrassment of riches. *Neuron* **44,** 5–21 (2004).
27. Yuste, R. & Bonhoeffer, T. Morphological changes in dendritic spines associated with long-term synaptic plasticity. *Annu. Rev. Neurosci.* **24,** 1071–1089 (2001).
28. Mu, Y. & Poo, M. M. Spike timing-dependent LTP/LTD mediates visual experience-dependent plasticity in a developing retinotectal system. *Neuron* **50,** 115–125 (2006).
29. Mooney, R., Madison, D. V. & Shatz, C. J. Enhancement of transmission at the developing retinogeniculate synapse. *Neuron* **10,** 815–825 (1993).
30. Ziburkus, J., Dilger, E. K., Lo, F. S. & Guido, W. LTD and LTP at the developing retinogeniculate synapse. *J. Neurophysiol.* **102,** 3082–3090 (2009).
31. Butts, D. A., Kanold, P. O. & Shatz, C. J. A burst-based "Hebbian" learning rule at retinogeniculate synapses links retinal waves to activity-dependent refinement. *PLoS Biol.* **5,** e61 (2007).
32. Shah, R. D. & Crair, M. C. Retinocollicular synapse maturation and plasticity are regulated by correlated retinal waves. *J. Neurosci.* **28,** 292–303 (2008).
33. Zhang, J., Ackman, J. B., Xu, H. P. & Crair, M. C. Visual map development depends on the temporal pattern of binocular activity in mice. *Nature Neurosci.* **15,** 298–307 (2011).
34. Liu, S. Q. & Cull-Candy, S. G. Synaptic activity at calcium-permeable AMPA receptors induces a switch in receptor subtype. *Nature* **405,** 454–458 (2000).
35. Cull-Candy, S., Kelly, L. & Farrant, M. Regulation of Ca^{2+}-permeable AMPA receptors: synaptic plasticity and beyond. *Curr. Opin. Neurobiol.* **16,** 288–297 (2006).
36. Isaac, J. T., Ashby, M. C. & McBain, C. J. The role of the GluR2 subunit in AMPA receptor function and synaptic plasticity. *Neuron* **54,** 859–871 (2007).
37. Goel, A. *et al.* Cross-modal regulation of synaptic AMPA receptors in primary sensory cortices by visual experience. *Nature Neurosci.* **9,** 1001–1003 (2006).
38. Hohnke, C. D., Oray, S. & Sur, M. Activity-dependent patterning of retinogeniculate axons proceeds with a constant contribution from AMPA and NMDA receptors. *J. Neurosci.* **20,** 8051–8060 (2000).
39. Jia, Z. *et al.* Enhanced LTP in mice deficient in the AMPA receptor GluR2. *Neuron* **17,** 945–956 (1996).
40. Toyoda, H. *et al.* Long-term depression requires postsynaptic AMPA GluR2 receptor in adult mouse cingulate cortex. *J. Cell. Physiol.* **211,** 336–343 (2007).
41. Needleman, L. A., Liu, X. B., El-Sabeawy, F., Jones, E. G. & McAllister, A. K. MHC class I molecules are present both pre- and postsynaptically in the visual cortex during postnatal development and in adulthood. *Proc. Natl Acad. Sci. USA* **107,** 16999–17004 (2010).
42. Stefansson, H. *et al.* Common variants conferring risk of schizophrenia. *Nature* **460,** 744–747 (2009).
43. Ripke, S. *et al.* Genome-wide association analysis identifies 13 new risk loci for schizophrenia. *Nature Genet.* **45,** 1150–1159 (2013).

Acknowledgements We thank members of the Shatz laboratory for helpful comments. For technical assistance, we thank N. Sotelo-Kury, C. Chechelski and P. Kemper. For training in retinogeniculate slice methods, we thank C. Chen, P. Kanold and D. Butts. This work was supported by NIH grants R01 MH071666 and EY02858, and the G. Harold and Leila Y. Mathers Charitable Foundation (C.J.S.); NIH grant RO1 EY13528 (M.B.F.); NDSEG and NSF Graduate Research Fellowships (J.D.A.); and an NSF Graduate Research Fellowship (L.A.K.).

Author Contributions H.L. and C.J.S. designed all experiments, analysed and reviewed all results and wrote manuscript. Data contributions are as follows: electrophysiology experiment by H.L.; multi-electrode array experiments by L.A.K. and M.B.F. B.K.B. designed H2-D^b monoclonal antibody and performed western blots. H.L. designed and performed RT–PCR experiments. A.D. performed RGC neuronal tract tracing experiments and analysis. J.D.A. and S.C. performed Taqman qPCR.

Author Information Reprints and permissions information is available at www.nature.com/reprints. The authors declare no competing financial interests. Readers are welcome to comment on the online version of the paper. Correspondence and requests for materials should be addressed to C.J.S. (cshatz@stanford.edu).

METHODS

All experimental protocols were approved by Stanford University Animal Care and Use Committees. K^bD^b-/- mice were provided by H. Ploegh[19] and $NSED^b$ mice by M. B. A. Oldstone[20]. These mice were maintained on C57BL/6 backgrounds. Crosses of these two lines generated $K^bD^{b-/-}$;$NSED^{b+}$ mice plus littermate controls. Electrophysiological recordings were made from LGN neurons by cutting parasagittal brain slices containing dorsal lateral geniculate nucleus (dLGN) and optic tract; synaptic transmission and degree of innervation was assessed as previously described[15]. For plasticity experiments at retinogeniculate synapses, perforated patch-clamp technique and induction protocols with natural activity patterns were used[31]. Multi-electrode array recordings of retinal waves and anatomical labelling of retinogeniculate projections to determine status of eye-specific segregation were carried out according to ref. 18 and ref. 14. Pharmacological investigation of CP-AMPA receptors was carried out according to ref. 34. All experiments were conducted and analysed blind to genotype except in Fig. 4 (genotype was obvious to experimenter because of phenotype). Sample sizes were chosen for each experiment to reach statistical significance (P value equal to or less than 0.05; details given in Methods and figure legends).

Genotyping. For $K^bD^{b-/-}$: three primer sets were mixed together (A: 5′-CGG AAGTCGCCTTACCTGATTG-3′, B: 5′-CAGCAGAAACATACAAGCTGTC-3′, C: 5′-GTCTCCTCTGGCACCTATGGG-3′), from which bands of 520 bp were detected for wild type, 400 bp for $K^bD^{b-/-}$ and double bands of 520 bp + 400 bp for heterozygote $H2\text{-}K^{b+/-}H2\text{-}D^{b+/-}$. For $NSED^b$ mice and $K^bD^{b-/-}$;$NSED^{b+}$: several primer sets were used, resulting in reliable and consistent results: a primer set consisting of $NSED^b$-A (5′-GAGATCGACTCTAGAGGATC-3′) and $NSED^b$-B1 (5′-GCGCTCTGGTTGTAGTAGCC-3′)[20] or $NSED^b$-B2 (5′-GTAGCCGAGCA GGTTCCTCA-3′) amplifies part of NSE promoter region and exon 2 of H2-D^b cDNA (~500 bp) (Extended Data Fig. 3b). Another primer set was designed to detect a unique D^b minigene expression cassette of ~800 bp (A: 5′-CGACACAGG GACGCTGACG-3′, B: 5′- CAGCTCCAATGATGGCCATAG-3). Taqman qPCR primer mix (H2-D1/H2-K1 (Mm04208017_mH) was also used, with same results.

Slice preparation. Parasagittal brain slices containing the dorsal lateral geniculate nucleus (dLGN) and optic tract were obtained as previously described[15,44]. The brain was removed rapidly and immersed in oxygenated ice-cold choline-based slicing solution (composition in mM: 78.3 NaCl, 23 $NaHCO_3$, 33.8 choline chloride, 2.3 KCl, 1.1 NaH_2PO_4, 6.4 $MgCl_2{\cdot}6H_2O$, 0.45 $CaCl_2{\cdot}2H_2O$, 23 glucose, aerated with 95% O_2/5% CO_2). The hemispheres were separated at an angle of 5–10° relative to midline. The larger hemisphere including optic tract was glued onto the cutting stage of a vibratome (Leica VT1000S) at an angle of 15–20°, which puts optic tract and LGN in the same plane relative to the blade; 250-μm-thick slices were cut. Note that only one slice per animal containing both intact optic tract and LGN can be obtained due to the small size of the LGN at relevant ages. Cortex was separated from thalamus to prevent excitatory recurrent disynaptic responses between dLGN and corticothalamic neurons. Slices were recovered at 31 °C for 30 min in choline chloride slicing solution, and then for 30 min in artificial cerebrospinal fluid (ACSF) (ACSF composition in mM: 125 NaCl, 26 $NaHCO_3$, 2.3 KCl, 1.26 KH_2PO_4, 1.3 $MgSO_4{\cdot}7H_2O$, 2.5 $CaCl_2{\cdot}2H_2O$, 25 glucose, aerated with 95% O_2/5% CO_2).

Electrophysiology. All recordings were at room temperature in a chamber with constant ACSF flow, except for paired-pulse ratio measurements, which were made at 30–32 °C. Stimulating electrode(s) were placed along the optic tract at the ventral end of dLGN and/or lateral edge of dLGN aligned with the recording site. dLGN neurons were distinguished by their large soma size and 3+ primary dendrites[15]. For synaptic current measurements, glass electrodes were filled with Cs^+-based internal recording solution (2–4 MΩ, composition in mM: 105 CsCl, 20 TEA-Cl, 2 $MgCl_2$, 1 EGTA, 10 HEPES, 3 Mg-ATP, 15 phosphocreatine, 1 Na-GTP, 5 QX-314, pH 7.4, 280 mOsm). To block inhibitory synaptic responses, SR95531 (20 μM; Tocris) or picrotoxin (100 μM; Sigma-Aldrich) was bath applied. AMPA receptors were blocked with DNQX (20 μM; Tocris), and NMDA receptors were blocked with DL-APV (100 μM; Tocris). For NMDA/AMPA ratio and spermine (0.1 mM, Sigma-Aldrich) dependent I_{AMPA} measurements, D600 (methoxyverapamil hydrochloride, 0.1 mM; Tocris) was added in Cs^+-based internal solution to block voltage-gated calcium channel activation. Spermine-containing internal solution was prepared fresh every 1–2 h. NASPM (1-naphthyl acetyl spermine trihydrochloride, 20–100 μM; Tocris) was bath applied. Rectification index was calculated by dividing peak I_{AMAP} at +40 mV with at −40 mV from I–V curves measured using spermine-containing internal solution[34].

For patch-clamp recordings: synaptic responses were recorded using an Axopatch 200B or 700A amplifier (Axon Instruments/Molecular Devices), digitized using Digidata 1322A (Axon Instruments) and data acquisition was performed by Clampex 9.2 (Axon Instrument). For whole-cell voltage clamp experiments, the series resistance (Rs) was corrected by 60–80% after cancellation of capacitive components. For synaptic plasticity experiments in which EPSC size was less than 120 pA, compensation was omitted. Calculated liquid junction potentials (Cs^+ internal: 4 mV; K^+ internal: 9 mV) were not compensated, except for spermine-dependent I–V relationship plots (Figs 4 and 5). Series resistance (Rs) was constantly monitored throughout experiments by injecting small hyperpolarizing currents.

For synaptic plasticity experiments: perforated patch-clamp technique was performed using a K^+-based internal solution containing amphotericin B (Fisher Scientific) (composition in mM: 115 K-methane Sulphonate, 20 KCl, 0.2 EGTA, 10 HEPES, 4 Mg-ATP, 10 phosphocreatine, 0.3 Na-GTP, pH 7.3 with KOH). Note that perforated patch recordings are necessary to prevent dialysis of intracellular components required for plasticity[29,31,45]. Amphotericin B stock solution (40–60 mg ml^{-1} in DMSO) was prepared fresh every day, from which 100–200 μg ml^{-1} internal solution was prepared hourly and kept on ice. The tip of the patch electrode was filled with internal solution without amphotericin B before back-filling with amphotericin B containing internal solution. Following the formation of GΩ seal, gradual drop of access resistance was monitored until stabilizing at 20–120 MΩ. Trials with sudden changes in Rs (clearly discernible due to rupture of perforation or clogging of patch pipette by amphotericin B precipitation) were discarded. EPSC changes with stable Rs within ±20 MΩ were used for analysis except when gradual changes in Rs were correlated with changes in EPSCs size. After obtaining a stable baseline for 10–20 min, the configuration was switched to current-clamp mode and plasticity induction protocols were applied by pairing optic tract stimulation with postsynaptic current injection for 1 s to generate 10–20 Hz action potentials either synchronously or with 1,100 ms latency (Fig. 3a–c)[31]. V_m (resting membrane potential measured at $I = 0$ configuration in perforated patch clamp mode) was not different between wild type (−58.5 ± 1.2 mV: $N = 16$ cells from 16 animals), $K^bD^{b-/-}$ (−59.6 ± 1.3 mV: $N = 10$), $K^bD^{b-/-}$;$NSED^{b+}$ (−60.5 ± 1.9 mV: $N = 13$) or $K^bD^{b-/-}$;$NSED^{b-}$ (−62.2 ± 2.5 mV: $N = 7$) ($P > 0.1$, t-test). The paring protocol was repeated 10 times over a 40 s interval. Data were acquired with resting membrane potentials (measured at $I = 0$) greater than −53 mV. For the NASPM LTD rescue experiments (Extended Data Fig. 8), 20 μM NASPM was added to the bath, and the asynchronous pairing protocol (10 times over a 40 s interval) was repeated twice, separated by 20 min. N = one cell per each animal. Percentage change is mean ± s.e.m. of EPSC amplitude averaged over 30 min after conditioning period as compared to baseline per cell.

For optic tract stimulation, concentric bipolar (CBABD70; FHC Inc.) or low-resistance glass-electrode filled with ACSF were used for stimulating electrodes without noticeable differences. Stimulus strength was regulated using an ISO-Flex stimulus isolator (A.M.P.I.) and applied at 0.025–0.033 Hz. For plasticity experiments, stimulus strength was set to achieve stable EPSCs (10–120 pA) activated by a single or a few fibres, and stimuli were applied at 0.025 Hz. To measure spermine-dependent I–V rectification, stimulation intensity was adjusted to evoke I_{AMPA} currents in the 100–300 pA range, due to the presence of Ca^{2+}-permeable AMPA receptor-mediated synaptic responses in $K^bD^{b-/-}$ mice.

Evaluation of the number of synaptic inputs. The number of connected fibres was estimated using two approaches modified from ref. 15. First, synaptic responses were recorded while varying optic tract stimulus intensity from minimal to maximal. Stimulation in increments of 1.0–2.5 μA was used between 0 μA and 100 μA, and larger increments (10–20 μA) were used at stimulation intensities greater than 100 μA. The stimulus-response profile provides an estimate of the number of RGC inputs to the cell. We also estimated the number of inputs to each LGN neuron based on the single-fibre AMPA current elicited at −70 mV by minimal stimulation as a per cent of the total current elicited by maximal stimulation for the same cell (Fibre fraction). For minimal stimulation, the method is based on the assumption that minimal stimulation elicits synaptic responses from only a single fibre in the optic tract (SF-AMPA). After a synaptic response was observed, the intensity of electrical stimulation was lowered to obtain a failure rate higher than 50% (20–50 repeats). Synaptic responses with an onset latency of <5 ms within a 1-ms window were regarded as direct, monosynaptic responses. The mean peak amplitudes of successful responses were taken as the strength of the single fibre synaptic response (SF-AMAP). Onset latency of SF-AMPA by minimal stimulation (estimated as time to reach 10% of peak I_{AMPA}) was not different between wild type, $K^bD^{b-/-}$, $K^bD^{b-/-}$;$NSED^{b-}$ or $K^bD^{b-/-}$;$NSED^{b+}$ (Extended Data Fig. 1c). For maximal stimulation, electrical stimulation was increased until the peak synaptic currents reached steady-state level (1–600 μA range). Fibre fraction was calculated as a ratio of single-fibre synaptic strength (SF-AMPA) to maximal synaptic strength (Max-AMPA) from the same cell (FF = SF/Max-AMPA per cell, %). The number of cells recorded per animal was limited to 4 for SF-AMPAs and Max-AMPA measurements.

Kinetics of EPSCs were measured as both the width at half-maximal EPSC amplitude (half-width), and decay time within 80–20% range of peak EPSCs using Clampfit.

Multi-electrode array recordings of retinal waves. Retinas were isolated from wild-type and $K^bD^{b-/-}$ mice and pieces of retina were placed retinal-ganglion-cell-side

down onto a 60-electrode multi-electrode array arranged in an 8 × 8 grid (excluding the four corners) with 10 μm diameter electrodes at 100 μm spacing (Multi Channel Systems)[1,3,46]. The retina was held in place with a weighted piece of dialysis membrane and superfused continuously with artificial cerebral spinal fluid (ACSF) containing (in mM): 119.0 NaCl, 26.2 $NaHCO_3$, 11 glucose, 2.5 KCl, 1.0 K_2HPO_4, 2.5 $CaCl_2$, and 1.3 $MgCl_2$. ACSF was oxygenated with 95% O_2 and 5% CO_2 and maintained at 32 °C, pH 7.4. Each preparation was allowed to equilibrate for 20 min before data acquisition. Spontaneous firing patterns were then recorded for 60 min. Voltage traces on each electrode were sampled at 20 kHz and filtered between 120 and 2,000 Hz. Events that crossed a spike threshold were sorted offline to identify single units using Plexon Offline Sorter software. Single units were identified by combining principal component analysis together with a valley-seeking algorithm and were inspected manually. The mean firing rate of all units throughout the recording was calculated and units with a mean firing rate less than 10% of overall mean firing rate were excluded from further analysis. Spike-sorted data were analysed in MATLAB (Mathworks). To identify bursts, a modified Poisson Surprise algorithm was used as described previously. Mean burst values for each retina were grouped according to age (P5–P8 and P10–P12) and genotype (wild type and $K^bD^{b-/-}$). Differences between means of different genotypes within each age group were evaluated for statistical significance using a *t*-test. To determine spatial properties of waves, a pair-wise correlation index, CI, was computed as a function of distance between two cells for all spikes in the recording, using a method described previously[3,46]. The correlation index gives a measure of the likelihood relative to chance that a pair of neurons fire together within a 100-ms time window. The distance between cells was approximated as the distance between the electrodes on which the activity of the cells was recorded. The cell pairs were grouped according to their intercellular distance, and medians were computed over all cell pairs in a given distance group for each individual retina. The median correlation indices were then averaged across retinas, for each age and genotype, and plotted as a function of intercellular distance.

Anterograde labelling of retinal ganglion axons and multiple threshold analysis. All methods were performed according to previously described studies[14,47]. P31–34 mice were anaesthetized with isoflurane. Cholera toxin B (CTB) subunit (1–2 μl) conjugated to AF488 was injected in the right eye and CTB subunit conjugated to AF594 was injected in the left eye (1 mg ml^{-1} dissolved in 0.2% DMSO, Invitrogen). After 24 h, animals were perfused and fixed by transcardial perfusion of 0.1 M phosphate buffered saline (PBS), then ice-cold 4% paraformaldehyde (PFA) in 0.1 M PBS. Brains were post-fixed in 4% PFA overnight. 100-μm-thick sections were cut on a freezing microtome. Sections were mounted with Prolong Antifade Gold (Invitrogen), and after coverslipping were imaged on a Zeiss Leica PS2 confocal microscope (Leica Microsystems). dLGN sections taken at the middle of the rostral-caudal extent of dLGN where the area of the ipsilateral eye projection is greatest were imaged in red and green channels. Images were acquired and analysed such that the peak intensity values were below maximum, and multiple threshold analysis was used by varying red and green channels at intensity thresholds of 20%, 40%, 60%, 80% and 100% of maximum. To measure the amount of overlap between inputs from both eyes, pixels overlapping in both red and green channels were identified using Image J (NIH) and the Colocalization plug-in tool. The total area of overlapping pixels was represented as a percentage of total dLGN area. Two-way ANOVA was used for statistical analysis.

RT–PCR. RNA was prepared from tissue using RNAqueous-4PCR (Ambion, Life Technologies) followed by cDNA synthesis using iScript Select cDNA synthesis kit (Bio-Rad). RT–PCR was performed using 0.5–1.0 μg of template cDNA using primers as follows (Extended Data Fig. 3b, c). H2-D^b: A, 5′-CAAGAGC AGTGGTTCCGAGTGAG-3′; B, 5′-CTTGTAATGCTCTGCAGCACCACT-3′. GAPDH (glyceraldehyde-3-phosphate dehydrogenase; used as a reference gene): A, 5′-ATTGTCAGCAATGCATCCTGC-3′; B, 5′-AGACAACCTGGTCCTCA GTGT-3′.

The quality of cDNAs was confirmed by genotyping PCR reactions using 0.5–1 μg of cDNA as template and the samples with genomic DNAs were discarded. H2-D^b-specific RT–PCR bands from $K^bD^{b-/-}$;$NSED^{b+}$ were confirmed by sequencing following cloning into pCR2.1-TOPO TA vector (Life Technology Corporation).

Taqman qPCR. RNA was extracted from each thalamus and cDNA was synthesized using iScript cDNA Synthesis kit (Bio-Rad). Gene expression was analysed with Taqman Gene Expression Assays (Applied Biosystems) for H2-D1/H2-K1 (Mm04208017_mH) and housekeeping gene GAPDH (Mm99999915_g1). All reaction mixes contained 5% 20× Taqman Gene Expression Assay, 50% Taqman Master Mix (4304437), 25% MilliQ water, and 200 ng of cDNA in 20 μl total volume per well. Experiments were carried out on a 7300 Real Time PCR system (Applied Biosystems). The relative amount of tested message was normalized to GAPDH, and efficiency corrected based on standard curves. Gene expression levels were normalized relative to wild-type control, which was set to 1. All samples were run in triplicate at least three times. Analyses were carried out as previously described using one-way ANOVA[48].

Immunoprecipitation/western blots of H2-D^b. Brain lysates in lysis buffer (150 mM NaCl, 50 mM Tris, 0.25% sodium deoxycholate, 1% NP-40, 1 mM EGTA, 1 mM PMSF, 1X Pefabloc (Roche)) were prepared by shearing ten times in a dounce homogenizer, then centrifuging at 12,000*g* for 10 min. Supernatants were precleared by incubation with Protein G-agarose beads (Invitrogen), and protein amounts were measured using a BioRad protein assay. Normalized lysates were then incubated with 12 μg anti-H2-D^b antibody 28-14-8 (BD Biosciences, 553600) overnight at 4 °C. Protein G-agarose was incubated with samples for 45 min. Beads were washed three times with lysis buffer, and then heated to 85 °C for 3 min in NuPAGE LDS 4× sample buffer (Invitrogen) + 1% β-2 mercaptoethanol. Samples were then electrophoresed on an SDS–PAGE gel, transferred to Immobilon-P PVDF transfer membrane (Millipore), and western blotted with rabbit monoclonal antibodies to H2-D^b, made against the extracellular domain of H2-D^b.

GluR1/2 expression levels. Thalami were isolated from P22 wild-type or $K^bD^{b-/-}$ mice, and synaptosome-enriched fractions prepared as described[49,50]. Freshly isolated individual thalami were homogenized in homogenization buffer (10 mM HEPES pH 7.3, 0.5 mM EGTA, 33% sucrose, 4 mM Pefabloc SC PLUS (Roche), and 0.2 mM phenylmethanesulphonyl fluoride (PMSF)), and centrifuged (10 min at 2,000*g*). Supernatants were passed through three layers of 100 μm pore nylon membranes, and then through 5 μm nitrocellulose filters. Filtrates were centrifuged (10,000*g* for 10 min), and pellets re-suspended in homogenization buffer. Protein amounts were determined by BioRad Protein Assay (BioRad) (about 200 μg synaptosomal protein was obtained per thalamus), and SDS–PAGE sample buffer (Novex) was added to a 1× concentration. After heating (85 °C for 4 min), equivalent amounts of protein from each sample (20 μg per sample) were electrophoresed on a SDS–PAGE gel, transferred to PVDF membrane (Bio-Rad), and western blotted with antibodies to GluR1 (Millipore, AB1504), GluR2 (Abcam, AB133477), N-tubulin (Abcam, AB18207), or GAPDH (Abcam, AB9485).

For quantification, gels were scanned and intensities of bands were quantified using the Image J program. After quantification, intensity values for GluR1 and GluR2 were normalized by dividing them against each GAPDH or N-tubulin values from the same thalamus. Western blots typically were run with multiple wild-type and $K^bD^{b-/-}$ samples; to compare results from different western blots, the intensity measurement for each sample thalamus was normalized against the average value derived from all wild-type bands on that same blot. The GluR1/GluR2 ratio for each thalamus was then determined. Finally, an average GluR1/GluR2 ratio was calculated from each individual thalami (Extended Data Fig. 7e).

Mouse cortical cultures were made as described[51]. Wild-type or $K^bD^{b-/-}$ cortical neurons were isolated at E16.5, and cultured on 6-cm tissue culture plates for 14 days *in vitro*. Plates were then washed twice with PBS and cells were lysed directly on the plates with lysis buffer (150 mM NaCl, 50 mM Tris-HCl pH 7.5, 0.25% sodium deoxycholate, 1% NP-40, 1 mM EGTA, 1 mM PMSF, 1× Pefabloc SC PLUS (Roche)) for 10 min. Lysates were then centrifuged at 12,000*g* for 10 min. Supernatants were normalized by BioRad Protein Assay (BioRad), and equivalent amounts of protein from each sample (25 μg per sample) were subjected to SDS–PAGE and western blotting with antibodies to GluR1, GluR2, GAPDH, and/or N-tubulin, as described above. Gels were scanned and bands quantified using Image J. Values were then normalized by dividing them by GAPDH or N-tubulin values, and an average GluR1/GluR2 ratio was calculated from each individual sample (Extended Data Fig. 7f). Non-parametric Mann–Whitney *U*-test (Prism software) was used to calculate *P* values for all analyses (two-tailed).

Data analysis and statistics for electrophysiology experiments. Data analysis as well as graph plotting were done using Clampfit 10.2 (Axon Instruments) and the OriginPro8.0 (OriginLab Corporation). Cages containing mice of different genotypes used for each experiment were relabelled and randomized so that experimenter did not know genotype. Experiments were then analysed blind to genotype unless stated in figure legends. In addition, Student's *t*-test was used for data with normal distribution and Mann–Whitney *U*-test for data with non-normal distribution. Shapiro–Wilk test was conducted for normality test. N = number of animals; n = number of cells. Average data are presented as mean ± s.e.m., unless stated otherwise. For synaptic plasticity experiments, *t*-test was used. Two-tailed analysis was used throughout the study.

44. Turner, J. P. & Salt, T. E. Characterization of sensory and corticothalamic excitatory inputs to rat thalamocortical neurones in vitro. *J. Physiol. (Lond.)* **510,** 829–843 (1998).
45. Rae, J., Cooper, K., Gates, P. & Watsky, M. Low access resistance perforated patch recordings using amphotericin B. *J. Neurosci. Methods* **37,** 15–26 (1991).
46. Torborg, C. L., Hansen, K. A. & Feller, M. B. High frequency, synchronized bursting drives eye-specific segregation of retinogeniculate projections. *Nature Neurosci.* **8,** 72–78 (2005).
47. Torborg, C. L. & Feller, M. B. Unbiased analysis of bulk axonal segregation patterns. *J. Neurosci. Methods* **135,** 17–26 (2004).

48. Adelson, J. D. *et al.* Neuroprotection from stroke in the absence of MHCI or PirB. *Neuron* **73,** 1100–1107 (2012).
49. Johnson, M. W., Chotiner, J. K. & Watson, J. B. Isolation and characterization of synaptoneurosomes from single rat hippocampal slices. *J. Neurosci. Methods* **77,** 151–156 (1997).
50. Yin, Y., Edelman, G. M. & Vanderklish, P. W. The brain-derived neurotrophic factor enhances synthesis of Arc in synaptoneurosomes. *Proc. Natl Acad. Sci. USA* **99,** 2368–2373 (2002).
51. Viesselmann, C., Ballweg, J., Lumbard, D. & Dent, E. W. Nucleofection and primary culture of embryonic mouse hippocampal and cortical neurons. *J. Vis. Exp.* (2011).

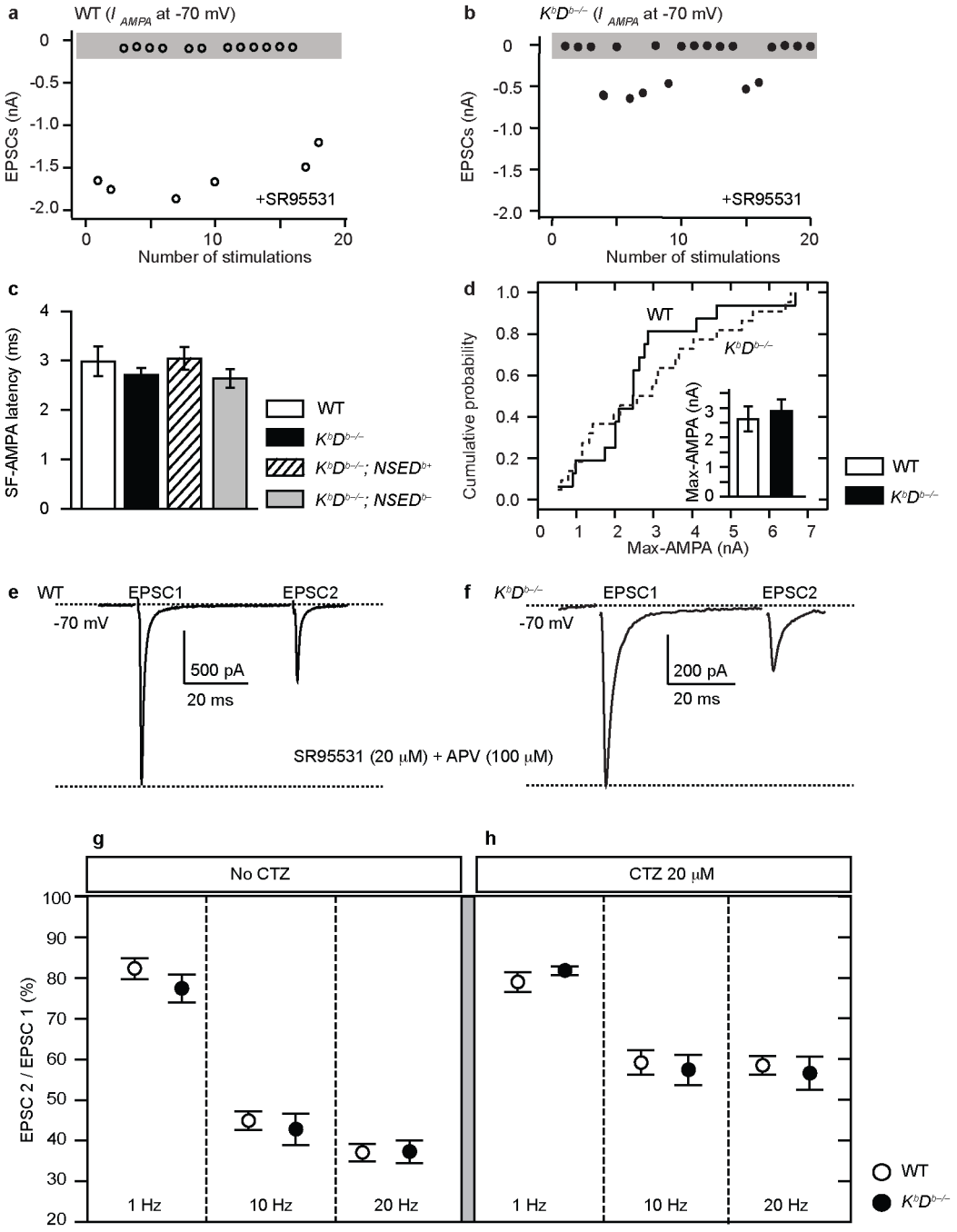

Extended Data Figure 1 | Comparison of retinogeniculate synaptic responses in wild type versus $K^bD^{b-/-}$. **a**, **b**, Examples of minimal stimulation for wild type (open circles) and $K^bD^{b-/-}$ (filled circles). Plot of EPSC peak versus number of stimulations (grey box represents failures, >50%). **c**, No difference in onset latency of SF-AMPA between all genotypes. Onset latency of SF-AMPA was estimated using minimal stimulation as time (ms) to reach 10% of peak I_{AMPA} from stimulation artefact (wild type: 3.0 ± 0.3 (n = 12 cells/N = 6 animals); $K^bD^{b-/-}$: 2.7 ± 0.1 (n = 23/N = 8); $K^bD^{b-/-}$;$NSED^{b+}$: 3.0 ± 0.2 (n = 17/N = 7); $K^bD^{b-/-}$;$NSED^{b-}$: 2.6 ± 0.2 (n = 19/N = 5); P > 0.5, t-test). **d**, Cumulative probability histogram shows no difference in Max-AMPA between wild type and $K^bD^{b-/-}$. Inset: mean ± s.e.m. Wild type: 2.6 ± 0.4 nA (n = 14/N = 6); $K^bD^{b-/-}$: 2.9 ± 0.4 nA (n = 22/N = 8); P > 0.1, Mann–Whitney U-test. **e**–**h**, Presynaptic release probability at $K^bD^{b-/-}$ retinogeniculate synapses is similar to wild type at P20–24. **e**, **f**, Examples of EPSCs evoked by paired-pulse stimulation of optic tract (20 Hz) recorded in whole-cell mode in individual LGN neurons from wild type (**e**) versus $K^bD^{b-/-}$ (**f**). **g**, **h**, Paired-pulse depression (PPD) (%) (EPSC 2/EPSC 1) over varying intervals. **g**, Wild type (open circle) versus $K^bD^{b-/-}$ (filled circle) without cyclothiazide (CTZ), a blocker of AMPA receptor desensitization. Wild type versus $K^bD^{b-/-}$: 1 Hz: 82.3 ± 2.6 (n = 10) versus 77.4 ± 3.4 (n = 8); 10 Hz: 44.9 ± 2.3 (n = 9) versus 42.8 ± 3.9 (n = 9); 20 Hz: 37. 1 ± 2.1 (n = 10) versus 37.3 ± 2.8 (n = 9) (P > 0.1 for each). **h**, Wild type (open circle) versus $K^bD^{b-/-}$ (filled circle) with CTZ (20 μM). Wild type versus $K^bD^{b-/-}$: 1 Hz: 79.0 ± 2.4 (n = 9) versus 81.8 ± 1.1 (n = 7); 10 Hz: 59.2 ± 3.0 (n = 8) versus 57.4 ± 3.7 (n = 7); 20 Hz: 58.5 ± 2.3 (n = 8) versus 56.6 ± 4.1 (n = 7) (P > 0.1 for each). N = 4 for wild type; N = 3 for $K^bD^{b-/-}$ for **g**, **h**. There was no significant difference in PPD between wild type and $K^bD^{b-/-}$, but note significant decrease of PPD +20 μM CTZ versus 0 μM CTZ application for both wild type and $K^bD^{b-/-}$ at 10 Hz and 20 Hz (P < 0.05). t-test. mean ± s.e.m. n = cells/N = animals.

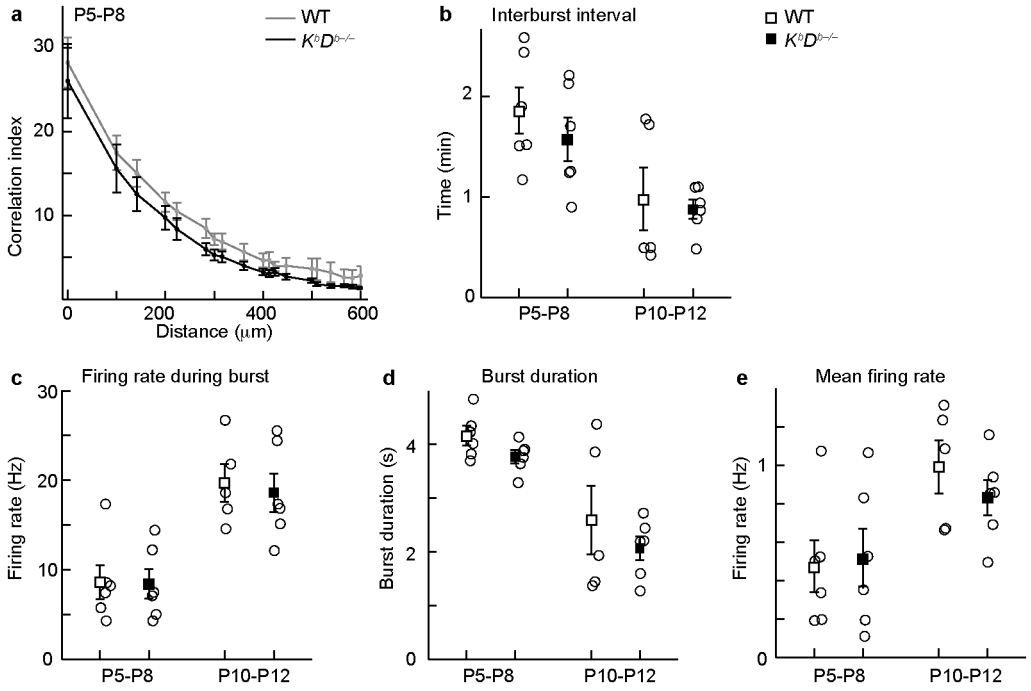

Extended Data Figure 2 | Intact spatio-temporal pattern of retinal waves in $K^bD^{b-/-}$ mice at P5–12. **a**, Correlation indices as a function of inter-electrode distance for all cell pairs for wild type (grey) and $K^bD^{b-/-}$ (black) at P5–P8. Data points correspond to mean values of medians from individual data sets and error bars represent s.e.m. **b**–**e**, Summary of temporal firing patterns for retinas isolated from wild-type (open squares) and $K^bD^{b-/-}$ (filled squares) mice at P5–P8 (stage II, cholinergic waves) and P10–P12 (stage III, glutamatergic waves). Open circles correspond to the mean values of individual retinas. **b**, Interburst interval for stage II (in min): wild type: 1.9 ± 0.2; $K^bD^{b-/-}$: 1.6 ± 0.2; stage III: wild type: 1.0 ± 0.3; $K^bD^{b-/-}$: 0.9 ± 0.1. **c**, Firing rate during burst for stage II (in Hz): wild type: 8.6 ± 1.9; $K^bD^{b-/-}$: 8.4 ± 1.7; stage III: wild type: 19.7 ± 2.1; $K^bD^{b-/-}$: 18.6 ± 2.2. **d**, Burst duration for stage II (in seconds): wild type: 4.2 ± 0.2; $K^bD^{b-/-}$: 3.8 ± 0.1; stage III: wild type: 2.6 ± 0.6; $K^bD^{b-/-}$: 2.1 ± 0.2. **e**, Mean firing rate for stage II (in Hz): wild type: 0.5 ± 0.1; $K^bD^{b-/-}$: 0.5 ± 0.2; stage III: wild type: 1.0 ± 0.1; $K^bD^{b-/-}$: 0.8 ± 0.1, mean ± s.e.m. ($P > 0.05$ for each, t-test, $N = 6$ animals for each group, except when $N = 5$ for stage III wild type; non-blind experiments).

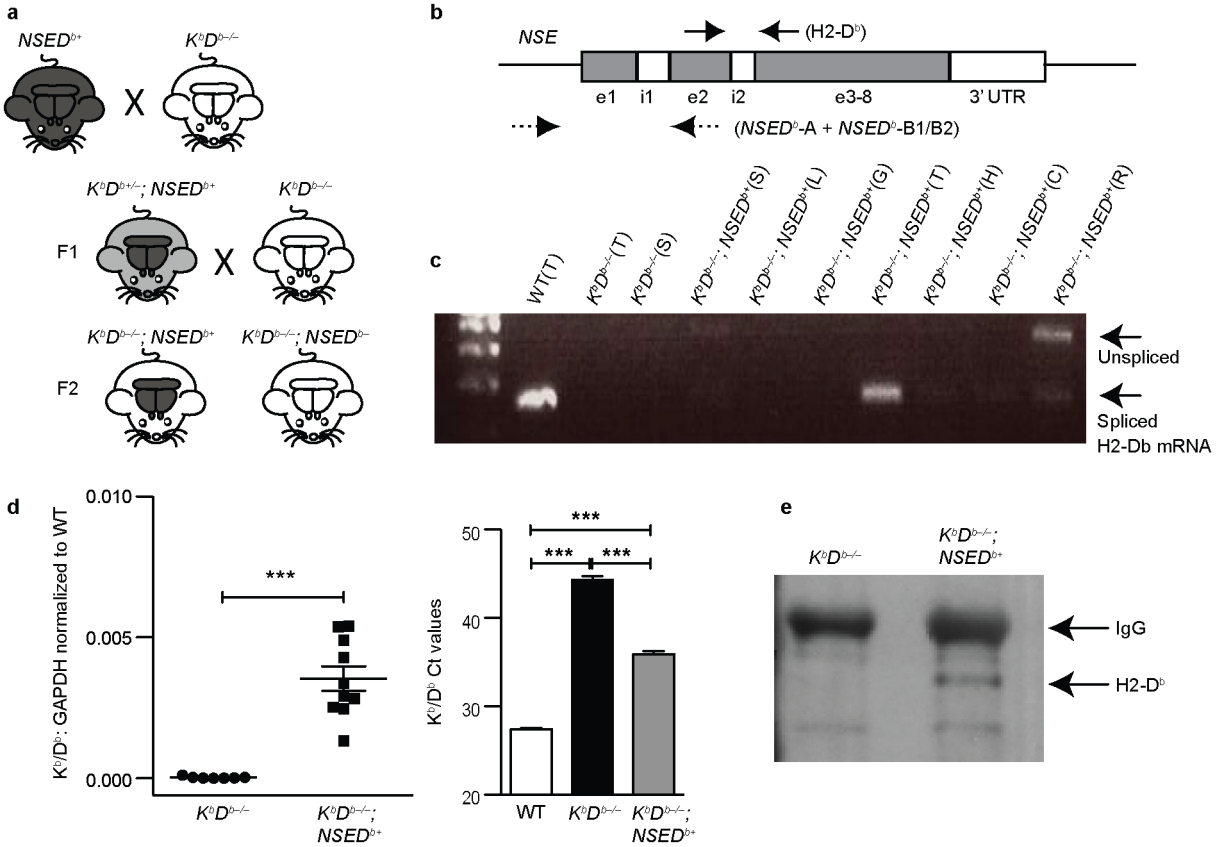

Extended Data Figure 3 | Rescue of H2-D^b expression in brain of $K^bD^{b-/-}$;$NSED^{b+}$ mice. **a**, Diagram of breeding strategy to generate $K^bD^{b-/-}$;$NSED^{b+}$ mice. $K^bD^{b-/-}$ (white indicates absence of H2-D^b) were crossed to $NSED^b$ transgenic mice (black indicates presence of H2-D^b in both body and brain). From F_1 offspring, $H2\text{-}K^{b+/-}H2\text{-}D^{b+/-}$;$NSED^{b+}$ mice (grey body, black brain) were selected and crossed to $K^bD^{b-/-}$ mice further, generating $K^bD^{b-/-}$;$NSED^{b+}$ (black brain with white body indicates rescue of H2-D^b expression in brain alone) and $K^bD^{b-/-}$;$NSED^{b-}$ littermate controls (white body, white brain). **b**, H2-D^b-specific primers. Solid arrows: forward (exon 2) and reverse (exon 3) for ~200 bp spliced mRNA as well as unspliced proRNA (~500 bp) (e; exon, i; intron). Dotted arrows: $NSED^b$-A (forward, NSE promoter region) and $NSED^b$-B1 and/or B2 (reverse, exon 2) for genotyping and mRNA detection[20]. **c**, RT–PCR showing rescue at P10 in thalamus of $K^bD^{b-/-}$;$NSED^{b+}$ mice cDNAs. Wild-type thalamus (WT(T)) shown as positive control; $K^bD^{b-/-}$ thalamus ($K^bD^{b-/-}$ (T)) and spleen ($K^bD^{b-/-}$ (S)) as negative controls, and various organs from $K^bD^{b-/-}$;$NSED^{b+}$ mice (spleen (S), liver (L), gut (G), thalamus (T), hippocampus (H), cortex (C), retina (R)) were used as templates. **d**, Quantitative PCR comparing relative H2-K^b/H2-D^b gene expression in wild type, $K^bD^{b-/-}$ and $K^bD^{b-/-}$;$NSED^{b+}$ thalami. Left: results show small but highly significant rescue of $H2\text{-}D^b$ mRNA expression in $K^bD^{b-/-}$;$NSED^{b+}$ ($K^bD^{b-/-}$: 0.00003 ± 0.00002; $K^bD^{b-/-}$;$NSED^{b+}$: 0.0035 ± 0.00044 relative to wild type: 1.0056 ± 0.032, $^{***}P = 0.0001$). Each point represents average relative gene expression for one mouse. Right: raw H2-K^b/H2-D^b Ct values for each genotype (wild type: 27.4 ± 0.1; $K^bD^{b-/-}$: 44.3 ± 0.4; $K^bD^{b-/-}$;$NSED^{b+}$: 35.9 ± 0.3; $^{***}P < 0.001$), one-way ANOVA, mean ± s.e.m. $N = 5$ animals for wild type, 7 for $K^bD^{b-/-}$, 10 for $K^bD^{b-/-}$;$NSED^{b+}$. **e**, Rescue of H2-D^b protein in $K^bD^{b-/-}$;$NSED^{b+}$ brains at P60. Western blot of immunoprecipitation from whole brain (three pooled brains) lysate from $K^bD^{b-/-}$ and $K^bD^{b-/-}$;$NSED^{b+}$. H2-D^b-specific signal from $K^bD^{b-/-}$;$NSED^{b+}$ appears below IgG band.

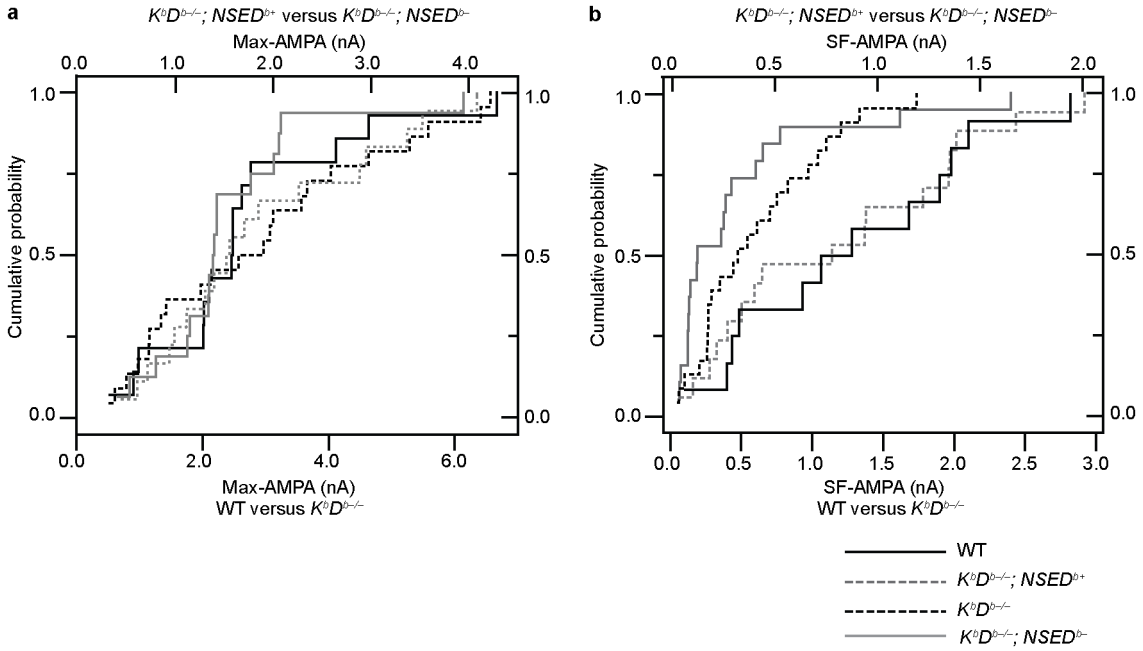

Extended Data Figure 4 | Cumulative probability distribution for SF-AMPA and Max-AMPA recorded at retinogeniculate synapses according to *H2-D*^{b} genotype. **a**, **b**, Max-AMPA (**a**) and SF-AMPA (**b**) showed similar cumulative probability histograms between wild type (black line), $K^bD^{b-/-}$;$NSED^{b+}$ (dashed grey line), $K^bD^{b-/-}$ (dashed black line) and $K^bD^{b-/-}$;$NSED^{b-}$ (grey line). Number of experiments are the same as in the main text, except for Max-AMPA: for $K^bD^{b-/-}$;$NSED^{b-}$: $n = 18$ cells/$N = 5$ animals; for $K^bD^{b-/-}$;$NSED^{b+}$: $n = 16/N = 7$ ($P > 0.05$, Mann–Whitney *U*-test). Fibre fraction calculated from Max-AMPA and SF-AMPA measurements is similar between wild-type and $K^bD^{b-/-}$;$NSED^{b+}$ mice (Fig. 2d).

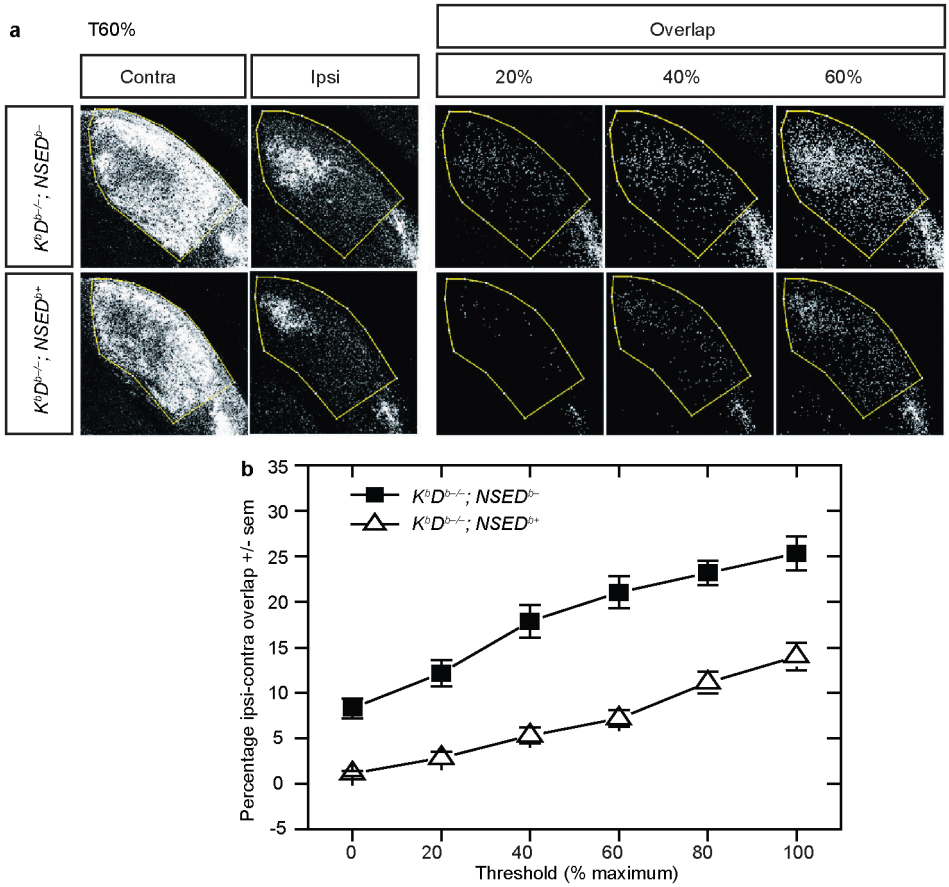

Extended Data Figure 5 | Neuronal H2-D^b expression in $K^bD^{b-/-}$ mice rescues impaired eye-specific axonal segregation at P34. a, Coronal sections of dLGN of $K^bD^{b-/-}$;$NSED^{b-}$ (top row) and $K^bD^{b-/-}$;$NSED^{b+}$ (rescue; bottom row) showing pattern of RGC axonal projections from the two eyes after intraocular tracer injections of CTB AF594 (red channel; contralateral eye injected) or AF488 (green channel; ipsilateral eye injected). Left: thresholded fluorescent images of dLGN at 60% maximum signal intensity (see Fig. 2e). Right: overlap of RGC projections (white pixels) from ipsilateral and contralateral eyes displayed for 20%, 40% and 60% maximal threshold for $K^bD^{b-/-}$;$NSED^{b-}$ (top) and $K^bD^{b-/-}$;$NSED^{b+}$ (bottom). Overlap = pixels labelled in both red and green channels. **b**, Mean percentage dLGN area ± s.e.m. pixel overlap for $K^bD^{b-/-}$;$NSED^{b-}$ (filled squares; $N = 3$) versus $K^bD^{b-/-}$;$NSED^{b+}$ (open triangles; $N = 4$): 0% threshold: 8.3 ± 1.1 versus 1.2 ± 0.3; 20% threshold: 12.2 ± 1.5 versus 2.9 ± 0.7; 40% threshold: 17.9 ± 1.8 versus 5.3 ± 0.9; 60% threshold: 21.1 ± 1.8 versus 7.2 ± 0.9; 80% threshold: 23.2 ± 1.3 versus 11.1 ± 1.2; 100%: 25.3 ± 1.9 versus 14.0 ± 1.5 ($P < 0.05$, two-way ANOVA). See Methods and ref. 47.

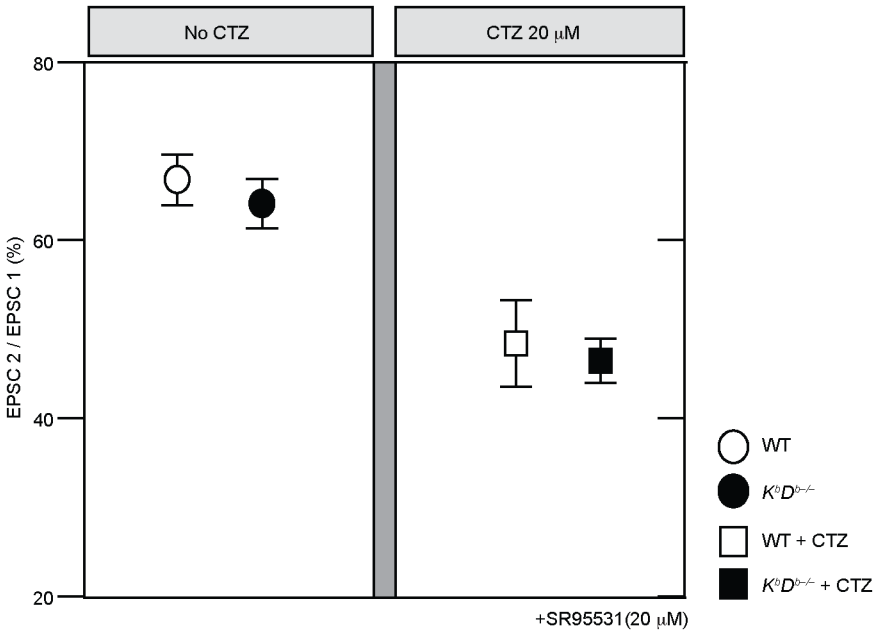

Extended Data Figure 6 | Intact release probability at $K^bD^{b-/-}$ retinogeniculate synapses before eye opening. Paired-pulse stimulation was delivered to the optic tract at 10 Hz, similar to the natural firing frequency of RGCs (Extended Data Fig. 2c), and whole-cell recordings were made from LGN neurons in slices aged between P8–13. Paired-pulse stimulation resulted in synaptic depression, represented as EPSC 2 divided by EPSC 1 (%). In 0 μM CTZ (left panel): wild type: 67.0 ± 2.9 ($n = 11/N = 4$); $K^bD^{b-/-}$: 64.2 ± 2.8 ($n = 7/N = 2$). In 20 μM CTZ (right panel): wild type: 48.6 ± 4.9 ($n = 8/N = 3$); $K^bD^{b-/-}$: 46.6 ± 2.5 ($n = 7/N = 2$) ($P > 0.1$ for each, *t*-test), mean ± s.e.m. 20 mM BAPTA containing Cs^+-internal solution was used for this experiment due to prolonged kinetics of EPSCs in $K^bD^{b-/-}$. The identical paired-pulse ratios between wild type and $K^bD^{b-/-}$ are consistent with the conclusion that presynaptic release probability is intact at P8–13 retinogeniculate synapses in $K^bD^{b-/-}$ mice. (See also Extended Data Fig. 1e–h for similar conclusion at P20–24, after synapse elimination is largely complete.)

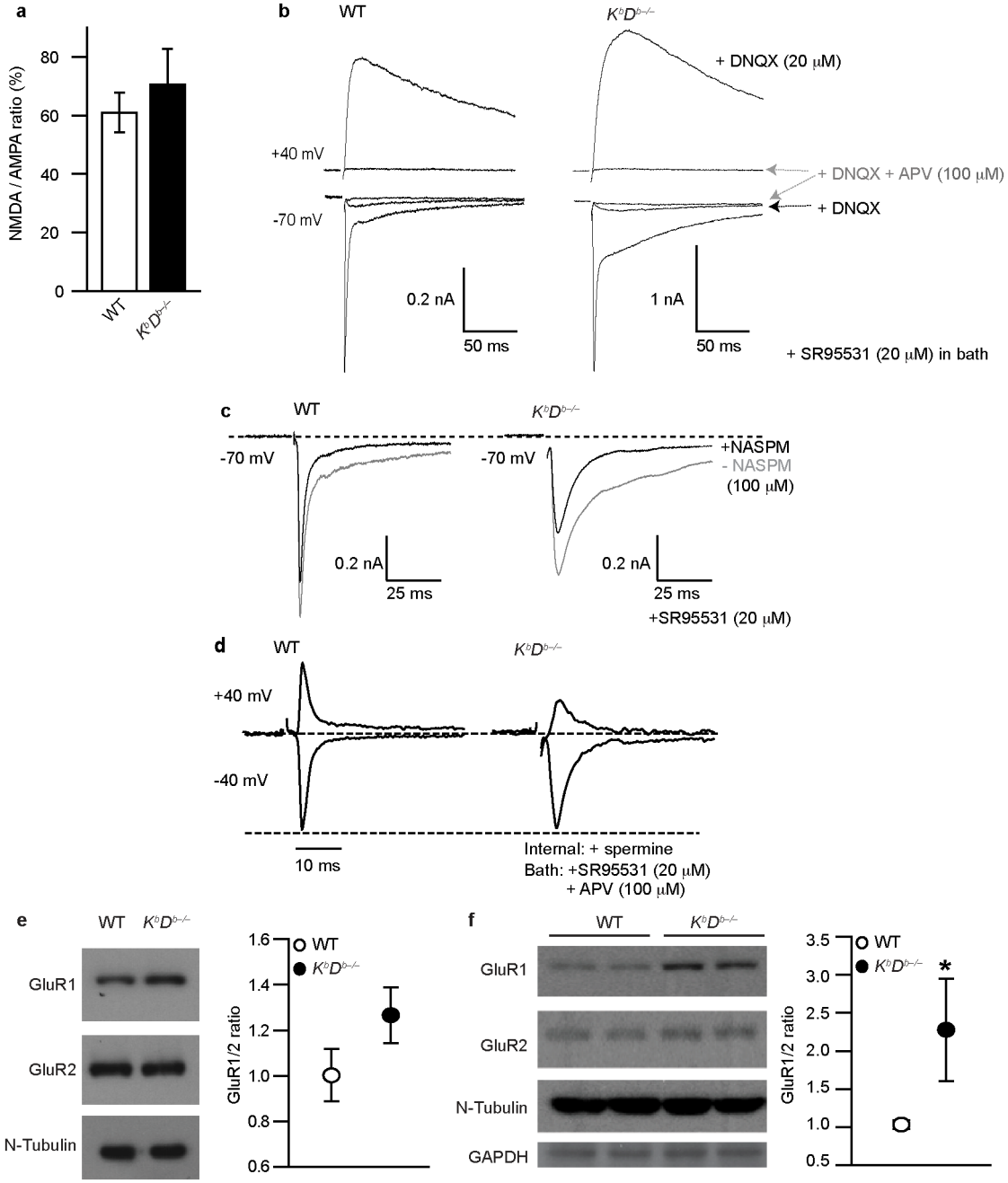

Extended Data Figure 7 | Normal NMDA/AMPA ratio but increased Ca^{2+}-permeable AMPA receptors at retinogeniculate synapses in $K^bD^{b-/-}$ mice. **a**, **b**, NMDA/AMPA ratio is unchanged in $K^bD^{b-/-}$ mice. **a**, NMDA/AMPA ratio (%): peak I_{AMPA} measured at −70 mV (+20 μM SR95531) versus peak I_{NMDA} at +40 mV (+20 μM SR95531 + 20 μM DNQX): wild type: 61 ± 6.8 ($n = 10/N = 4$); $K^bD^{b-/-}$: 70.6 ± 12.1 ($n = 7/N = 3$) ($P > 0.1$, t-test) mean ± s.e.m. **b**, Example recordings from individual neurons for wild type (left) and $K^bD^{b-/-}$ (right). APV (100 μM) was added at the end of each experiment to confirm NMDA-mediated synaptic currents. D600 in pipette. **c**, Example showing effect of NASPM (100 μM bath) on I_{AMPA}: note significant blockade of I_{AMPA} in $K^bD^{b-/-}$. Grey line, before NASPM; black line, after NASPM (5 traces averaged for single cell). SR95531 (20 μM) added to bath for **a**–**c**. **d**, Examples for I_{AMPA} normalized to EPSC amplitude at −40 mV. Note reduction in EPSC amplitude at +40 mV in $K^bD^{b-/-}$ but not wild type. 100 μM APV + 20 μM SR95531 in bath. Spermine (100 μM) and D600 (100 μM) in pipette. Ages: P8–13. Experimenter was aware of genotype due to obvious differences in time course of EPSCs and effects of NASPM. **e**, Example western blot (left) and GluR1/GluR2 ratio (right) of P22 thalamus; wild type: 1.0 ± 0.1 ($N = 12$); $K^bD^{b-/-}$: 1.3 ± 0.1 ($N = 13$) ($P = 0.07$). **f**, Example western blot (left) and GluR1/GluR2 ratio (right) of cultured cortical neurons; wild type: 1.0 ± 0.1 ($N = 4$); $K^bD^{b-/-}$: 2.3 ± 0.7 ($N = 4$) (*$P = 0.03$). Mann–Whitney U-test for **e**, **f**, n = cells/N = animals.

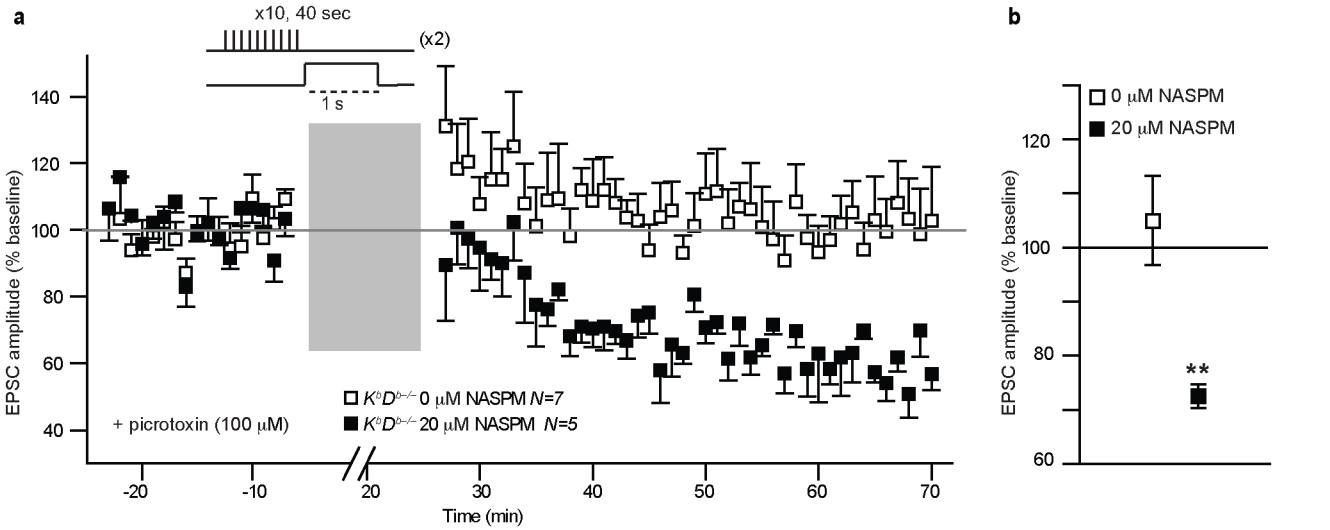

Extended Data Figure 8 | NASPM-dependent rescue of LTD in $K^bD^{b-/-}$ LGN at P8–13. **a**, Summary of all 1,100 ms latency experiments: EPSC peak amplitude (% change from baseline) versus time ($n = 7/N = 7$ for 0 μM NASPM; $n = 5/N = 5$ for 20 μM NASPM). Grey bar = induction period (Methods). 1 min data binning. **b**, Average of per cent change (mean ± s.e.m.); $K^bD^{b-/-}$ 0 μM NASPM: 105 ± 8.2 ($N = 7$); $K^bD^{b-/-}$ +20 μM NASPM: 72.5 ± 2.2 ($N = 5$). $^{**}P < 0.01$, *t*-test, *n* = cells/*N* = animals.

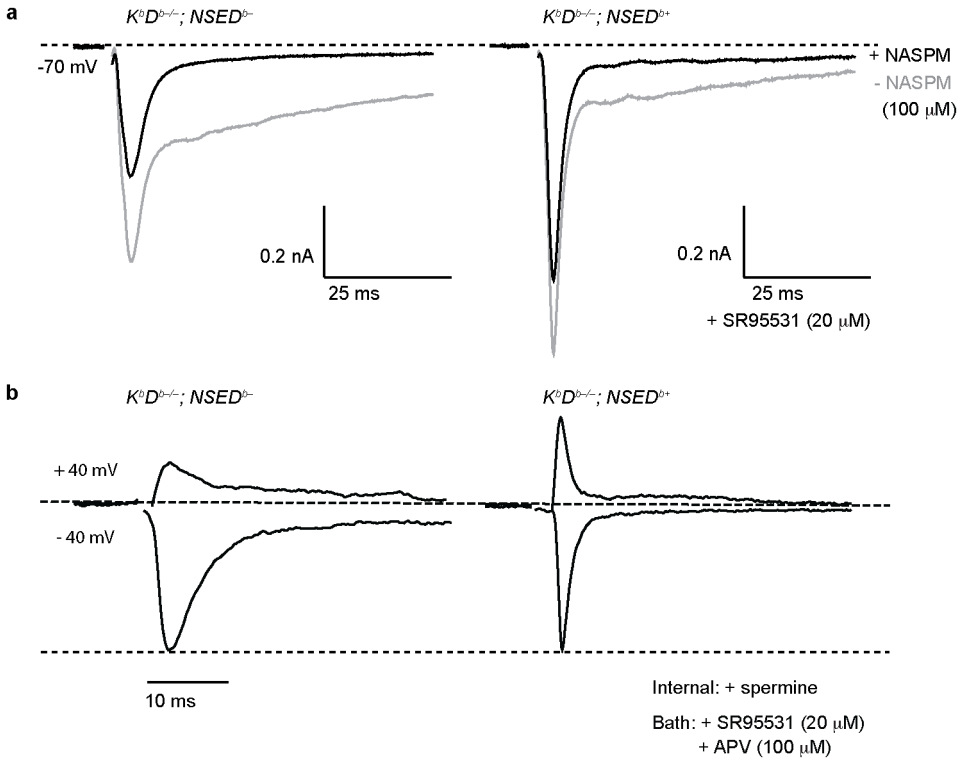

Extended Data Figure 9 | Neuronal H2-D^b expression decreases Ca^{2+} permeability of AMPA receptors at retinogeniculate synapses in $K^bD^{b-/-}$;$NSED^{b+}$ mice. **a**, NASPM blockade of I_{AMPA} is significantly reduced in $K^bD^{b-/-}$;$NSED^{b+}$ mice. Example trace of NASPM effect on I_{AMPA} recorded from $K^bD^{b-/-}$;$NSED^{b-}$ (left) or $K^bD^{b-/-}$;$NSED^{b+}$ (right) individual LGN neuron. Grey line, before NASPM; black line, after NASPM application (5 traces averaged for single cell); 20 μM SR95531 in bath. **b**, Internal spermine-dependent block of I_{AMPA} at positive membrane potentials is rescued in $K^bD^{b-/-}$;$NSED^{b+}$ LGN neurons. Example recordings for I_{AMPA} normalized to EPSC amplitude at −40 mV from individual neurons. Note reduction in EPSC amplitude at +40 mV in $K^bD^{b-/-}$; $NSED^{b-}$, but restored to wild-type level in $K^bD^{b-/-}$;$NSED^{b+}$. 100 μM APV + 20 μM SR95531 in bath. Spermine (100 μM) and D600 (100 μM) in internal solution.